Spiral waves of excitation underlie reentrant activity in isolated cardiac muscle.

A M Pertsov, J M Davidenko, R Salomonsz, W T Baxter and J Jalife

Circ Res. 1993;72:631-650
doi: 10.1161/01.RES.72.3.631
Circulation Research is published by the American Heart Association, 7272 Greenville Avenue, Dallas, TX 75231

Print ISSN: 0009-7330. Online ISSN: 1524-4571

Spiral Waves of Excitation Underlie Reentrant Activity in Isolated Cardiac Muscle

Arkady M. Pertsov, Jorge M. Davidenko, Remy Salomonsz, William T. Baxter, and José Jalife

The mechanism of reentrant ventricular tachycardia was studied in computer simulations and in thin (≈20×20×0.5-mm) slices of dog and sheep ventricular epicardial muscle. A two-dimensional matrix consisting of 96×96 electrically coupled cells modeled by the FitzHugh-Nagumo equations was used to analyze the dynamics of self-sustaining reentrant activity in the form of elliptical spiral waves induced by premature stimulation. In homogeneous anisotropic media, spirals are stationary and may last indefinitely. However, the presence of small parameter gradients may lead to drifting and eventual termination of the spiral at the boundary of the medium. On the other hand, spirals may anchor and rotate around small discontinuities within the matrix. Similar results were obtained experimentally in 10 preparations whose electrical activity was monitored by means of a potentiometric dye and high-resolution optical mapping techniques; premature stimulation triggered reproducible episodes of sustained or nonsustained reentrant tachycardia in the form of spiral waves. As a rule, the spirals were elongated, with the major hemiaxis parallel to the longitudinal axis of the cells. The period of rotation (183±68 msec [mean±SD]) was longer than the refractory period (131±38 msec) and appeared to be determined by the size of the spiral's core, which was measured using a newly devised "frame-stack" plot. Drifting of spiral waves was also observed experimentally. Drift velocity was 9.8% of the velocity of wave propagation. In some cases, the core became stationary by anchoring to small arteries or other heterogeneities, and the spiral rotated rhythmically for prolonged periods of time. Yet, when drift occurred, spatiotemporal variations in the excitation period were manifested as a result of a Doppler effect, with the excitation period ahead of the core being 20±6% shorter than the excitation period behind the core. As a result of these coexisting frequencies, a pseudoelectrocardiogram of the activity in the presence of a drifting spiral wave exhibited "QRS complexes" with an undulating axis, which resembled those observed in patients with torsade de pointes. The overall results show that spiral wave activity is a property of cardiac muscle and suggest that such activity may be the common mechanism of a number of monomorphic and polymorphic tachycardias. (*Circulation Research* 1993;72:631–650)

KEY WORDS • **reentry** • **ventricular tachycardia** • **torsade de pointes** • **Doppler effect** • **drifting spirals**

Reentrant excitation may lead to exceedingly rapid, self-sustaining, regular or irregular activity throughout the heart, which is the hallmark of life-threatening arrhythmias such as ventricular tachycardia and ventricular fibrillation.[1,2] Recent experimental studies[3–7] support the hypothesis[8–11] that reentrant excitation in ventricular muscle may be the result of spiral wave activity. This mechanism does not depend on any peculiarities of the cardiac muscle and may be demonstrated in any excitable medium. For example, spiral waves may be observed in the so-called Belousov-Zhabotinsky reaction (Winfree[12] and Muller et al[13]), as well as during the formation of multicellular aggregates in the social ameba,[14] the spreading depression in the retina of birds,[15] and the propagation of calcium waves in the cytosol of *Xenopus* oocytes.[16] In the case of the heart, the spiral wave concept may be complementary to more traditional ideas that are based on the classical notion of circus movement reentry,[17–19] as well as on the more recently developed concepts of leading-circle[20–22] and anisotropic[23,24] reentry, in that it may provide new insight into the dynamic behavior of rotating waves in the heart and hopefully lead to diagnostic and therapeutic advances.

In this article we present direct evidence of spiral wave activity in isolated preparations of epicardial muscle by use of potentiometric dyes and optical mapping techniques. Numerical simulations using a simple model of a generic two-dimensional excitable medium were used to predict the global behavior of small pieces of ventricular epicardial muscle during repetitive activity. The study was undertaken to address the following specific issues: 1) the mechanisms of initiation of sustained and drifting spiral waves, 2) the ability to induce spiral wave activity in heterogeneous cardiac muscle by use of point stimulation from a single source, 3) the influence of anisotropy on the rotation period and the excitable gap, 4) the direct correlation of the behavior of the spiral wave activity with the gross anatomy of the

From the Department of Pharmacology, State University of New York Health Science Center at Syracuse.

Supported in part by grants PO1-HL39707 and RO1-HL29439 from the National Heart, Lung, and Blood Institute and a Grant-In-Aid from the American Heart Association.

Address for correspondence: Dr. Arkady M. Pertsov, Department of Pharmacology, SUNY Health Science Center at Syracuse, 766 Irving Avenue, Syracuse, NY 13210.

Received January 30, 1992; accepted November 30, 1992.

tissue, and 5) the possible electrocardiographic patterns that may be produced by drifting spirals and the relation of such patterns to the mechanisms of monomorphic and polymorphic ventricular tachycardias (e.g., torsade de pointes).

Materials and Methods

Computer Model

The standard approach to simulating electrical activity of cardiac cells is to use ionic models[25] that are based on differential equations devised originally by Hodgkin and Huxley. However, the huge complexity of these models makes any attempt at simulating wave propagation in large arrays of electrically connected cardiac cells an unrealistic computational exercise. Thus, at the risk of giving up quantitative accuracy in our numerical experiments, we have elected not to use an ionic model but the much simpler qualitative approximation provided by the FitzHugh-Nagumo (FHN)–type equations.[26–31] This enabled us to carry out simulations of wave propagation in generic excitable media and to provide testable predictions about cardiac muscle behavior at a relatively low computational cost.

Two-dimensional matrices consisting of large numbers (48×48 or 96×96) of electrically coupled cells were used for computer simulations. Each cell in a given matrix had four immediate neighbors, and in the excited state, current flowing from one cell to another was proportional to both the potential difference and the conductance between them.

In the FHN model, each cell is described by two quantities: the transmembrane potential U and a variable V that accounts for total slow ionic current. The equations are as follows:

$$C(\partial U/\partial t)=F(U)-V+I_{ex}+G_x(\partial^2U/\partial x^2)+G_y(\partial^2U/\partial y^2) \quad (1)$$

$$\partial V/\partial t=(U-V)/\tau(U) \quad (2)$$

Equation 1 describes the dynamics of an electrical potential on the membrane capacitance C due to transmembrane current F(U)−V, external current I_{ex}, and current through intercellular spaces described by the diffusion term $G_x(\partial^2U/\partial x^2)+G_y(\partial^2U/\partial y^2)$, where G_x and G_y are longitudinal and transverse conductances, respectively. Equation 2 describes the dynamics of slow ionic currents, where τ is the time constant. The condition $\partial U/\partial n=0$ ("impermeability" condition) was set for the boundary.

We used a piecewise linear function[28,29] F(U) and piecewise constant function $\tau(U)$ as follows:

$$\begin{aligned} F(U)&=-c_1U && \text{at} \quad U<e_1\\ &=c_2(U-a) && \text{at} \quad e_1<U<e_2\\ &=-c_3(U-1) && \text{at} \quad U>e_2 \end{aligned} \quad (3)$$

$$\begin{aligned} \tau(U)&=\tau_1 && \text{at} \quad U<b_1\\ &=\tau_2 && \text{at} \quad b_1<U<b_2\\ &=\tau_3 && \text{at} \quad U>b_2 \end{aligned} \quad (4)$$

The introduction of the voltage dependence of τ allowed us to decrease recovery time and thus to reduce computational cost by minimizing both the rotation period of a spiral wave and the necessary array size. A similar model has been used elsewhere[30,31] and shown to reproduce all of the main features of spiral wave dynamics. These two reasons determined our choice of the model even though the other FHN modifications (e.g., the model of van Capelle and Durrer[27]) may generate more realistic action potentials. Parameter values used in calculations of Equations 3 and 4 were similar to those that have been described previously,[29] namely, $c_1=4$, $c_2=0.95$, $c_3=15$, and $e_1=0.018$. The parameters a and e_2 are found from the continuity condition for F(U): $a=e_1(c_1/c_2)$ and $e_2=[(c_1+c_2)e_1+c_3]/(c_3+c_2)$. The following values are also used: $\tau_1=0.5$, $\tau_2=16.66$, $\tau_3=3.5$, $b_1=0.01$, and $b_2=0.95$.

Anisotropy (μ) was introduced as $\mu=G_x/G_y=1$, 4, 9, or 16, which resulted in a longitudinal-to-transverse conduction velocity ratio (anisotropic ratio [AR]) of 1.0, 2.0, 3.0, or 4.0; the latter ratio (AR=4) is equivalent to that observed experimentally in sheep epicardial muscle.[32]

To solve the differential equations (Equations 1–4) numerically, we used a simple Euler method of integration. The diffusion terms were evaluated by finite differences using the five-point formula

$$[U_{i-1,j}+U_{i+1,j}-2U_{i,j}+\mu(U_{i,j-1}+U_{i,j+1}-2U_{i,j})]/h^2 \quad (5)$$

where $U_{i,j}$ is the value of U at grid point (i, j).

The size of each grid element was $h_x=h_y=h=0.325$, and the time step was $h_t=0.03$. Programs were written in computer language C and run on a SPARC station (Sun Microsystems). Analysis was performed on a Zenith 386/25 computer using an Epix video imaging board. Video images of potential distribution in space U(x,y) were displayed as gray levels, with white being maximum excitation and black being complete rest. Hard copies were obtained on a Mitsubishi 3600 video printer.

We have used parameters derived from experimental results to scale our model. Accordingly, $\Delta U=1.0$ was related to 120 mV, $\Delta x=10.0$ to 5 mm, and $\Delta t=1.0$ to 8 msec.

Experimental Methods

The preparation. Young sheep and mongrel dogs were anesthetized with sodium pentobarbital (35 mg/kg i.v.). The hearts were rapidly removed and placed in warm, oxygenated Tyrode's solution. After clearly identifying the fiber orientation by gross anatomic inspection, square pieces of epicardial muscle (approximately 20×20×0.5 mm) were cut with a dermatome. Care was taken to avoid the regions of the main coronary arteries or any large bands of connective tissue. Suitable preparations were immediately transferred to a Plexiglas chamber (40×40×6 mm) and pinned to the wax floor of the chamber mounted on an antivibration table. The tissues were continuously superfused (20 ml/min) with Tyrode's solution containing (mM) NaCl 130, KCl 4, $NaHCO_3$ 24, NaH_2PO_4 1.2, $MgCl_2$ 1, $CaCl_2$ 1.8, and glucose 5.6. Solutions were bubbled with 95% O_2–5% CO_2 (pH 7.4, 37±0.5°C).

For the optical recording of the membrane potential, the preparations were stained with the voltage-sensitive dye di-4-ANEPPS (Molecular Probes, Inc., Eugene, Ore.; 13 μg/ml). Application of the dye was carried out 1 hour after tissue equilibration by continuous superfusion of a recirculating volume (1,000 ml) of the dye-containing Tyrode's solution. The dye was allowed to bind for three 5-minute periods, with subsequent washout with dye-free Tyrode's solution. To avoid mechanical artifacts induced by the contractions of the preparations, di-acetyl-monoxime (DAM, 15 mM) was added to the superfusate before the beginning of the optical recordings. To rule out the contribution of this agent in the generation of the arrhythmia, in seven experiments, self-sustained activity was also generated before the addition of DAM to the superfusate, and the activity was monitored by means of intracellular microelectrodes.

Optical recording techniques. The light from a tungsten-halogen lamp was collimated and made quasimonochromatic by use of an interference filter (490 nm) together with a heat filter (model KG-3, Schott Glass Technologies, Inc., Duryea, Pa.) The light was then reflected 90° from a dichroic mirror (560 nm) and focused onto the preparation. A 50-mm objective lens was used to collect the emitted light. The depth of field of our optical system was approximately 12 mm. The emitted light was transmitted through the emission filter (645 nm) and projected onto a photodiode array or a video camera.

Photodiode system. We used a 10×10 photodiode array (RC Centronics). The output of each photodiode was connected to a current-to-voltage converter and then to one of seven 16-channel A/D boards (RC Centronics). Each of the 100 channels was sequentially digitized (12 bits) with a time resolution of 1 msec per channel and stored on a 40-megabyte hard disk. After processing the data, the signals were visualized on a storage oscilloscope (Tektronix, Beaverton, Ore.) as snapshots of fluorescence from the whole array or as plots of fluorescence versus time from selected photodiodes. Detailed description of the electronics is provided elsewhere.[4,6]

Video camera system. A CCD solid-state video camera (Cohu series 6500) with more than 360,000 picture elements was used. The video images (typically, 400×200 pixels) were acquired with a 4-megabyte A/D frame-grabber board (Epix) in a noninterlace mode with a speed of 60 frames per second (16.66 msec per frame). The board was mounted in a Zenith 386/20 computer and was used to digitize the analog signal from the camera and to process the imaged data. To reveal the signal, the background fluorescence was subtracted from each frame. Low-pass filtering was applied to improve the visualization of signals. Individual frames were convolved with a cone-shaped kernel. The half height of the kernel triangular cross section corresponded to approximately 0.4–0.5 mm (effective spatial resolution) on the preparation. No temporal averaging was used. An RGB color monitor (model PVM 13420, Sony) was used to display the images.

Stimulation protocol. The preparations were stimulated through a coaxial bipolar electrode (point stimulation) or one of four pairs of Ag/AgCl lateral electrodes embedded into the wax bottom of the chamber.[4,6,7] For lateral stimulation, each pair of the electrodes was long enough (20 mm) to stimulate almost the entire length of one edge of the preparation. Action potential duration and refractory period were determined using conventional techniques during stimulation at a basic cycle length (BCL) of 300 msec and at a BCL similar to that found during reentrant activity. Conduction velocities in the longitudinal and transverse directions were defined from the optical recordings during point stimulations (BCL, 300 msec) as the distance traveled by the elliptical wave front along the main hemiaxes over time.

Standard S_1-S_2 stimulation protocols were used for the induction of the reentrant arrhythmia in the experimental preparation. One of two different modalities was used: 1) standard S_1-S_2 point stimulation through a coaxial bipolar silver electrode and 2) cross-field stimulation.[3,4,6,7,9,33] Briefly, in the case of cross-field stimulation, the basic stimulus (S_1) was applied through one of the lateral electrodes (BCL, 300 msec; pulse duration, 5 msec; pulse amplitude, 1.5 to two times threshold). Premature stimulation (S_2) was applied perpendicularly through a different lateral electrode (S_1-S_2 interval, variable; S_2 duration, 5–10 msec; intensity, two to five times threshold). A pair of Pulsar 6i stimulators (Frederick Haer Co.) was used as the stimulation source. A third stimulator was used for synchronization of the optical mapping system to allow for monitoring of the initiation of spiral wave activity. In most experiments, transmembrane potentials were continuously recorded using glass microelectrodes filled with 3 M KCl and connected to a dual microprobe system (model 700, World Precision Instruments, New Haven, Conn.).

Simulated electrocardiogram. Two "electrocardiographic" leads (D_x and D_y) were obtained from both experimental preparations and computer simulations. For the experiments, the electrocardiogram was calculated as follows: 1) Each video frame was divided into two halves (i.e., left and right for the horizontal lead, D_x). 2) At each point in time (i.e., one video frame), the average transmembrane voltage activity (i.e., the change in fluorescence intensity) obtained from all pixels in one half of the frame was calculated. 3) The same value was calculated from the opposite half. 4) These two values were then subtracted from each other according to the expression $D_x=\Sigma E_{left}-\Sigma E_{right}$, where ΣE represents the sum of the pixel values from the left and right halves of the frame. The vertical lead D_y was calculated according to the expression $D_y=\Sigma E_{top}-\Sigma E_{bottom}$, where the subscripts top and bottom represent the corresponding halves of the frame. The same procedure was used for computer simulations in which the transmembrane potential is represented by the variable U.

Results

Stationary Spirals

Computer simulations.

INITIATION OF SPIRAL WAVES. Methods used to initiate rotating waves in the simulations as well as in the experiments (see below) are presented in Figure 1. In the case of cross-field stimulation (panel A), a conditioning stimulus S_1 ($I_{ex}=2\times$threshold), applied to the entire column of cells on the left border of the array, initiated a planar wave that propagated at a uniform

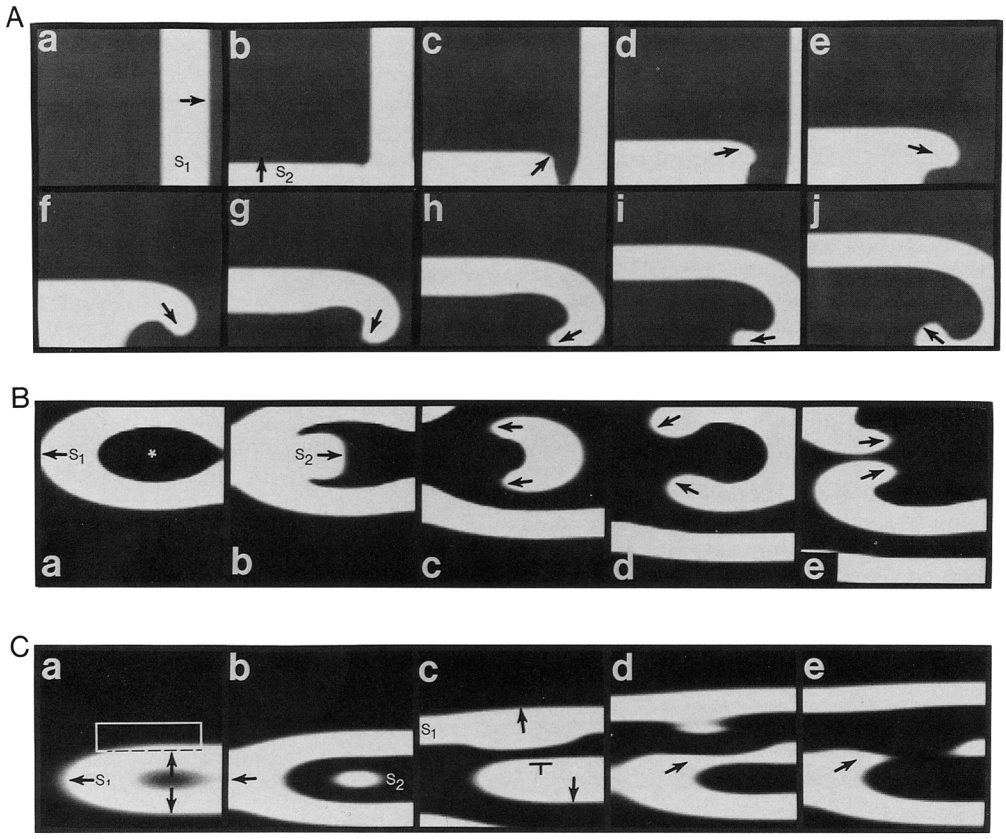

FIGURE 1. *Video frames showing the initiation of spiral wave activity in a two-dimensional array of 96×96 FitzHugh-Nagumo excitable cells. White represents excitation, and black represents resting potential. Arrows indicate the direction of the wave front. Panel A: Cross-field stimulation method (homogeneous and isotropic array): frame a, basic (S_1) planar wave propagates from left to right; frame b, premature (S_2) planar wave is initiated perpendicularly from the bottom border of the array; frame c, the S_2 wave front breaks into the refractory tail of S_1 and develops a pronounced curvature; frames d–j, the wave front curls and a clockwise rotating spiral is initiated. Frame to frame intervals are 16 msec for frames a–e and 24 msec for frames f–j. Panel B: Point stimulation method (different S_1 and S_2 application site; homogeneous array; anisotropic ratio, 2.0): frame a, S_1 stimulation (asterisk) produces elongated wave (the fast axis is horizontal); frame b, S_2 wave is initiated 14 pixels to the left of the S_1 stimulation site (the S_2 wave front breaks into the S_1 refractory tail); frame c, S_2 fails to propagate in the antegrade direction and forms two wave breaks with pronounced curvature, giving rise to a pair of counterrotating (figure-of-eight) spirals (frames d and e). Frame to frame interval is 8 msec for frames a and b and 32 msec for frames b–e. Panel C: Point stimulation (same location for S_1 and S_2; anisotropic ratio, 3.0). A rectangular patch of 12×32 elements with prolonged recovery time (τ_3=128 msec) was introduced in the central part of the array: frames a and b, S_1 and S_2 waves are shown; frame c, propagation patterns of S_1 and S_2 are shown. The prolongation of depolarization phase of S_1 prevents upward propagation of S_2 wave in the center of the array; frame d, S_2 breaks into the refractory tail of S_1; frame e, S_2 develops a wave break with a pronounced curvature giving rise to a spiral wave. Time delays between frames are 16, 32, 24, and 8 msec, respectively.*

velocity toward the right (see frame a). A test stimulus S_2 (I_{ex}=5×threshold), applied perpendicularly to S_1, initiated a second planar wave that propagated upward, except at the right, where it collided with the refractory tail of S_1 (frames b and c). This led to a break (a discontinuity) of the S_2 wave, which began to curl toward the right (frames c and d). In frames d–j, we present the subsequent evolution of the S_2 wave as it underwent a period of clockwise rotation and thereafter continued to rotate indefinitely (not shown). Thus, it should be possible to induce self-sustaining reentrant activity in a piece of two-dimensional excitable medium by producing a transient discontinuity in the propagating wave, even in the absence of anatomic or functional obstacles (for review, see References 8, 9, and 27).

The timing of the S_2 stimulus affected the location of both the break formation and the center of rotation of the spiral wave. Consequently, increasing the S_2 delay shifted the spiral center progressively to the right (not shown). At relatively long delays, the wave break occurred at a point that was too close to the right border of the array for the spiral to form. Moreover, the vulnerable interval (i.e., the interval during which premature stimulation resulted in spiral wave activity) was proportional to the conduction time of the S_1 wave and thus depended on the anisotropic ratio. In fact, the vulnerable interval was wider when S_1 propagated across and S_2 propagated along the main axis of the fibers.

The mechanism of spiral initiation using point stimulation with S_1 and S_2 applied to different sites is shown in Figure 1B. S_1 was applied at the point indicated by the asterisk in frame a. The elliptical wave front is the result of the anisotropy of the array (see below). The S_2

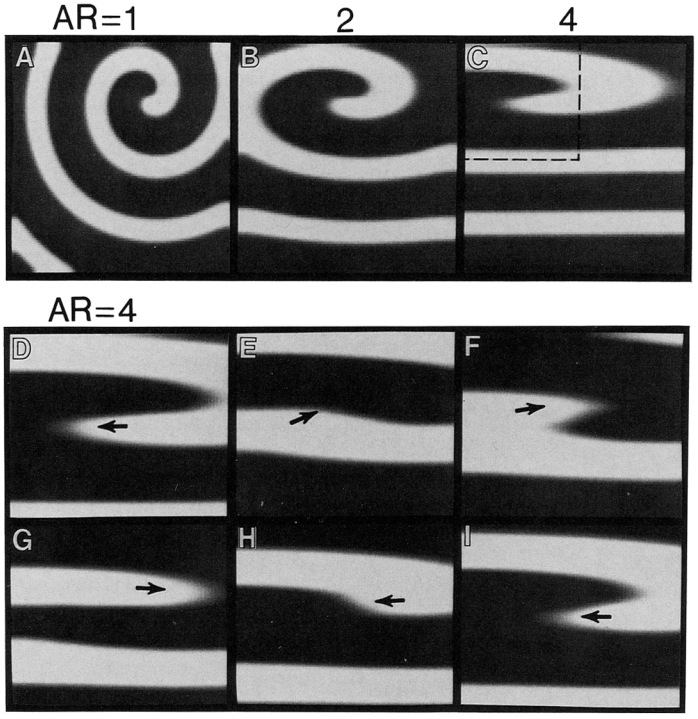

FIGURE 2. *Video frames showing simulated stationary spiral wave activity using three different degrees of anisotropy. Panel A: Anisotropic ratio (AR)=1. Panel B: AR=2. Panel C: AR=4. Panels D–I: Snapshots obtained during one complete cycle of the spiral wave shown in panel C. Only the central region of the spiral (indicated by the box of panel C) is displayed. Time delays between frames are 24 msec. Arrows indicate the direction of the wave front.*

stimulus was applied just to the left of the S_1 site at the time when the region was not yet completely recovered from the S_1 wave (frame b). As a result, the S_2 wave propagated only through recovered regions (frames c and d), giving rise to a pair of self-sustaining counter-rotating spirals.

To create a wave break necessary for spiral wave formation using point S_1-S_2 stimulation at a single site, a rectangular area with prolonged recovery time was introduced in the central part of the array (Figure 1C). This resulted in local prolongation of the depolarization phase of the S_1 wave (see frame c). S_2 failed to propagate into the refractory region and developed a wave break with a pronounced curvature, which initiated the rotating spiral (frames d and e).

Spirals waves were similar regardless of the method of stimulation or the degree of anisotropy (for the anisotropic ratio [AR] in Figure 1, panel A<panel B<panel C). In fact, the spiral in panel A had the same rotation period as in panel B. However, the vulnerable interval was longer for cross-field stimulation than for either type of point stimulation; thus, it was the most convenient and reproducible way to initiate spirals. Since our main goal was to study the dynamics of stationary and drifting spirals, regardless of the method of their initiation, the cross-field stimulation was adopted in the majority of computer simulations and experimental studies.

ISOTROPIC AND ANISOTROPIC SPIRALS. Figure 2 shows individual snapshots obtained from three different simulations in which the AR was increased from 1 (panel A) to 2 (panel B) and then to 4 (panel C). Clearly, in all cases, the excitation wave front has the shape of a stationary spiral that rotates rhythmically and periodically in a self-sustaining manner. Introducing anisotropy into the model changes the shape of the spiral from circular (panel A) to elliptical (panels B and C) and leads to spatial differences in the width of the excited region. However, in the model, anisotropy does not alter the period of rotation (T_s, 180 msec) nor the duration of the refractory tail at any point within the matrix (see below). This is not surprising, since introducing anisotropy into the model is topologically equivalent to simply stretching the matrix on one axis (e.g., x>y). Thus, in the case of cardiac muscle experiments, the model predicts that if wave propagation is, for example, approximately four times faster in the longitudinal than in the transverse direction, then an elongated spiral should be demonstrable whose major to minor hemiaxis ratio is approximately 4:1 (see panel C).

In heart muscle, the wave length (refractory period×conduction velocity) is relatively long. Thus, only a partial aspect of the spiral would be expected to be seen in a 20×20×0.5-mm slice of ventricular epicardial tissue (see below). In Figure 2, panels D–I are computer results for which individual frames are taken sequentially during a complete cycle of the magnified central part of the matrix (see dashed box in panel C). Note that, in any given frame, the excited state (white region) occupies a variable but finite space, which suggests the existence of a large excitable gap. The sequence of activation recorded at various points of the same anisotropic matrix during spiral wave activity is illustrated in Figure 3. In panel B, the individual "action potentials" (variable U) recorded from the sites indicated by the small letters in panel A demonstrate the existence of a typical reentry pattern.[22] Measurements of refractory period in the model using the S_1-S_2 protocol (two pulses starting from quiescence) resulted in a T_s/T_r ratio of approximately 1.5, where T_r is the refractory period. Thus, one may conclude that there is a significant excitable gap that is independent of the location of the recording site (e.g., compare sites a and c). Hence, as predicted by these simulations, even though anisotropic propagation leads to directional differences in the instantaneous spatial distribution of

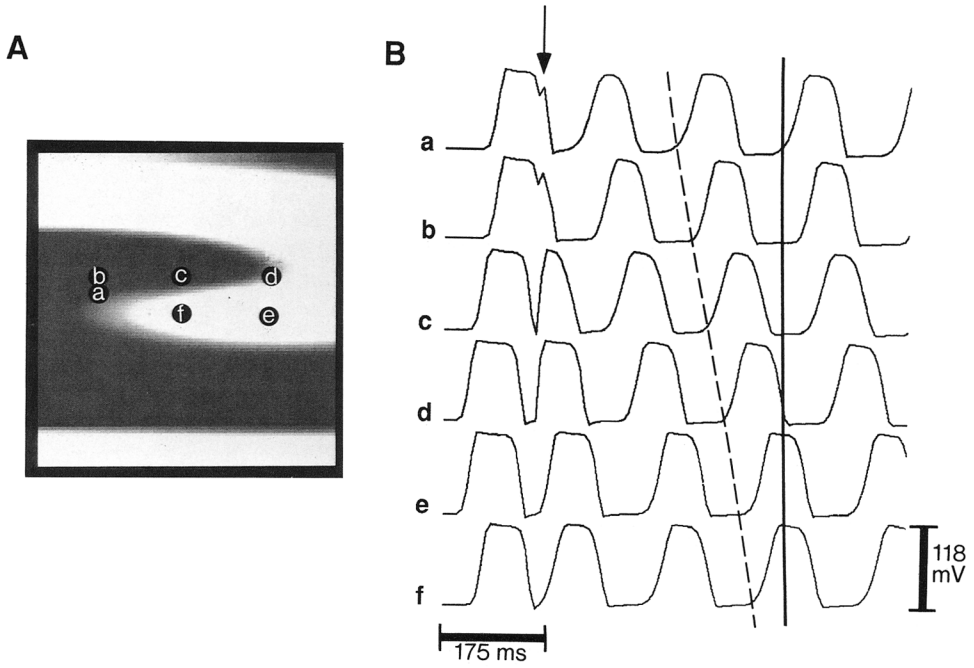

FIGURE 3. *Sequence of activation for the first four cycles of a clockwise rotating spiral wave. Panel A: Snapshot of spiral wave activity. The letters a–f indicate the location of the points selected for the recording of the action potentials. Panel B: Action potentials. In each tracing, the first response is the action potential induced by basic stimulus S_1. The arrow indicates the moment of S_2 delivery; the dashed line indicates the sequence of activation; and the solid line indicates the instant at which the snapshot of panel A was obtained.*

the excited state and the excitable gap, the duration of both parameters should remain independent of whether propagation is proceeding in the *x* or *y* direction. Moreover, the overall period of rotation should not be affected by the degree of anisotropy.

THE CORE OF THE SPIRAL. The theory of excitable media predicts that in the center of a spiral there should always be a small area of unexcited but excitable tissue, the "core," which determines all the major dynamic properties of the rotating activity[30]: the period of rotation, the duration of the excited state, and the duration of the excitable gap. The shape, size, voltage structure, and activity of the core of a stationary anisotropic spiral wave (AR=4.0) are shown in Figure 4. In panel A, the outline of the core is superimposed on the activity recorded for a single frame. In this simulation, the core is an elliptical domain at the center of rotation. The region surrounded by the ellipse representing the core is the area at which the maximum potential during one complete rotation is lower than 80% of the absolute maximum potential. The action potentials recorded at various points across the core region (as indicated in panel A) during the initial eight rotations after the initiation of spiral wave activity are presented in panel B. A pronounced shift in action potential time course is observed between points that are located at opposite sides of the core (see vertical line and compare tracings a and e). In addition, at the very center, the steady-state amplitude of the oscillations is extremely small, and full repolarization never occurs. This is more clearly apparent in panel C, in which the spatial distribution as well as the profiles of maximum potentials are shown. The amplitude decreases gradually toward the center of the core. As expected by the 4:1 anisotropy ratio, the transition is much more gradual in the horizontal direction than in the vertical direction.

Experimental results.

SPIRAL WAVES INITIATED BY POINT STIMULATION. In a series of three experiments, several episodes of spiral wave activity were induced by means of point stimulation, with S_1 and S_2 being applied at the same point. Figure 5 shows one example. The first frame on the top left shows the video image of the preparation and the bipolar electrode on the central surface of the tissue. The wave initiated by an S_1 stimulus (0 msec) propagated outward (16 msec), eventually activating the whole preparation (not shown). The duration and length of the tail of repolarization of S_1 were not uniform. In fact, at 176 msec a region in the upper right quadrant remained depolarized and thus refractory to any new activation. Consequently, a premature wave front (S_2) initiated 20 msec earlier from the same electrode was unable to propagate through that region. However, at 240 msec, the wave front began to curve (see arrow) and then to invade the region of prolonged refractoriness from the top downward (288 msec), which initiated a self-sustaining clockwise vortexlike activity with a rotation period of 115 msec (frames, 240–352 msec). These results support the numerical prediction (see Figure 1C) that the presence of intrinsic heterogeneities in the electrophysiological properties of the tissue (e.g., regions of prolonged refractoriness or regions of impaired conduction) sets the stage for the initiation of spiral wave activity by point stimulation, with S_1 and S_2 being applied from the same source.

ANISOTROPIC SPIRALS IN CARDIAC MUSCLE. Additional qualitative predictions derived from the computer simulations were tested in the isolated tissue experiments.

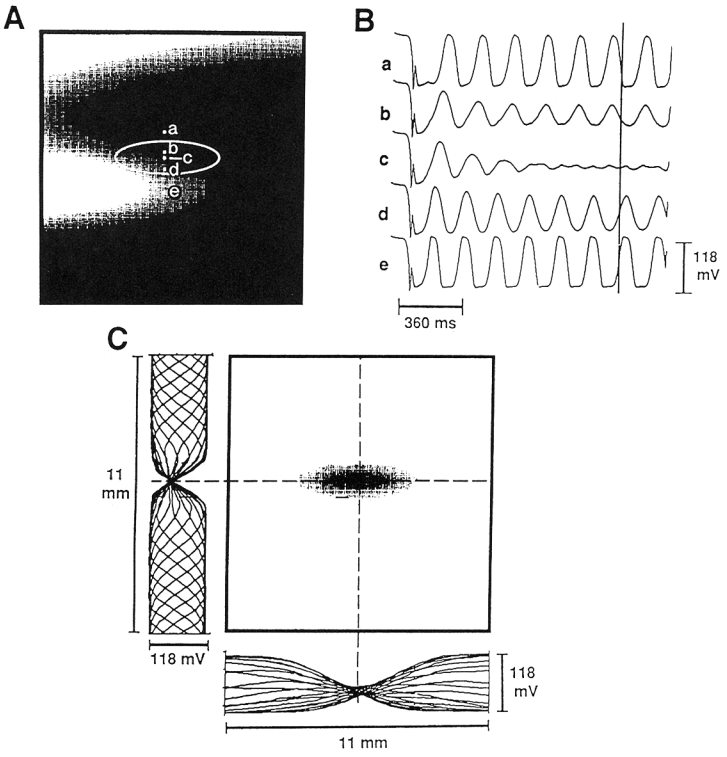

FIGURE 4. *Activity and voltage structure of the core area by computer simulation. Panel A: Counterclockwise rotating spiral wave obtained in an anisotropic array (the fast axis is horizontal). The core is an elliptical domain at the center of the array with the long axis parallel to the fast axis of the cells. The letters a–e represent points across the core selected for the recording of action potentials. Panel B: Individual pixel recordings obtained from the points indicated in panel A. The vertical line shows the instant at which the snapshot of panel A was obtained. Panel C: Voltage structure of the core. White is maximum and black is minimum voltage amplitude. Profiles of membrane potential were obtained once every 8 msec from the horizontal (bottom) and vertical (left) lines crossing the center of the core during one complete rotation.*

For example, as in the numerical results, cross-field stimulation consistently and reproducibly resulted in spiral wave activity. Indeed, stationary spiral wave activity occurred in a total of 33 episodes in all 10 preparations studied using this method.

Panel A of Figure 6 contains a series of video images taken from a sheep ventricular preparation during a single rotation of a wave that circulated repetitively and rhythmically in the clockwise direction with a constant period of 170 msec. The tip of a highly elongated spiral wave can be clearly seen in different sequential positions. In each frame, the activity resembles that obtained for the anisotropic spiral in the computer simulations presented in the preceding section (see Figures 2C–2I). Indeed, as a consequence of the high degree of anisotropy (longitudinal/transverse conduction velocity=[25.5 cm/sec]/[4.2 cm/sec]=6), the spiral was stretched in the longitudinal direction of the cell bundles. In addition, as predicted by the simulation, anisotropy led to directional differences in the instantaneous spatial distribution of the apparent excited state and excitable gap. However, as shown in panel B, within the limitations of our signal-to-noise ratio, the individual fluorescence signals recorded from selected sites of the preparation suggest that the duration of the diastolic interval was unaffected by the direction of propagation. Moreover, when aligned properly, these signals clearly show the typical sequence of activation observed in cardiac tissues during the reentry process.[22]

In 10 preparations, the anisotropic ratio was 3.64±2.2 (mean±SD; range, 1.57–6.8), which is similar to that reported previously for epicardial muscle.[32,34,35] The wide range in the anisotropic ratio of our preparations may be attributed to the fact that individual slices were not always cut from the same epicardial site. However, the shape of the spiral wave correlated well with the degree of anisotropy, being more elongated in preparations with a higher anisotropic ratio. The period of rotation varied from 97 to 205 msec in dog preparations and from 117 to 250 in sheep preparations; the T_s/T_r ratio was 1.35 in dog and 1.39 in sheep experiments, which indicated that in all cases the activity demonstrated a substantial excitable gap.

THE SHAPE OF THE CORE. Single video frames obtained during spiral wave activity in three experiments with different anisotropic ratios are presented in Figure 7. The core, represented in each panel by the dashed area, was measured by the method shown in Figure 4C (cutoff level, 30% of maximum fluorescence change). As predicted by the numerical simulations of anisotropic matrices, the cores were elliptical, with their long hemiaxes oriented parallel to the longitudinal fiber direction (all panels were oriented such that the fibers run horizontally). The values for the major and minor hemiaxes were, respectively, 2.75 and 1.75 mm for panel A, 2.75 and 1.37 mm for panel B, and 11 and 2 mm for panel C. In addition, the long axis/short axis ratio (L/S) corresponded closely with AR. The values for panels A, B, and C are as follows: L/S=1.57, AR=1.57; L/S=2, AR=2.7; and L/S=5.5, AR=6, respectively.

As in the computer simulations (see Figure 4), the amplitude of the fluorescence decreases gradually toward the center of the core. The voltage structure of the core is shown in Figure 8 as recorded by means of the video camera (panel A). Fluorescence at the very center was 35% of maximum fluorescence recorded at the periphery. In 10 episodes, the mean value of fluorescence at the center was 25±17% of the maximum. Action potentials displayed on the right show decreasing amplitude toward the center, and they have double component upstrokes at the very center of the core.

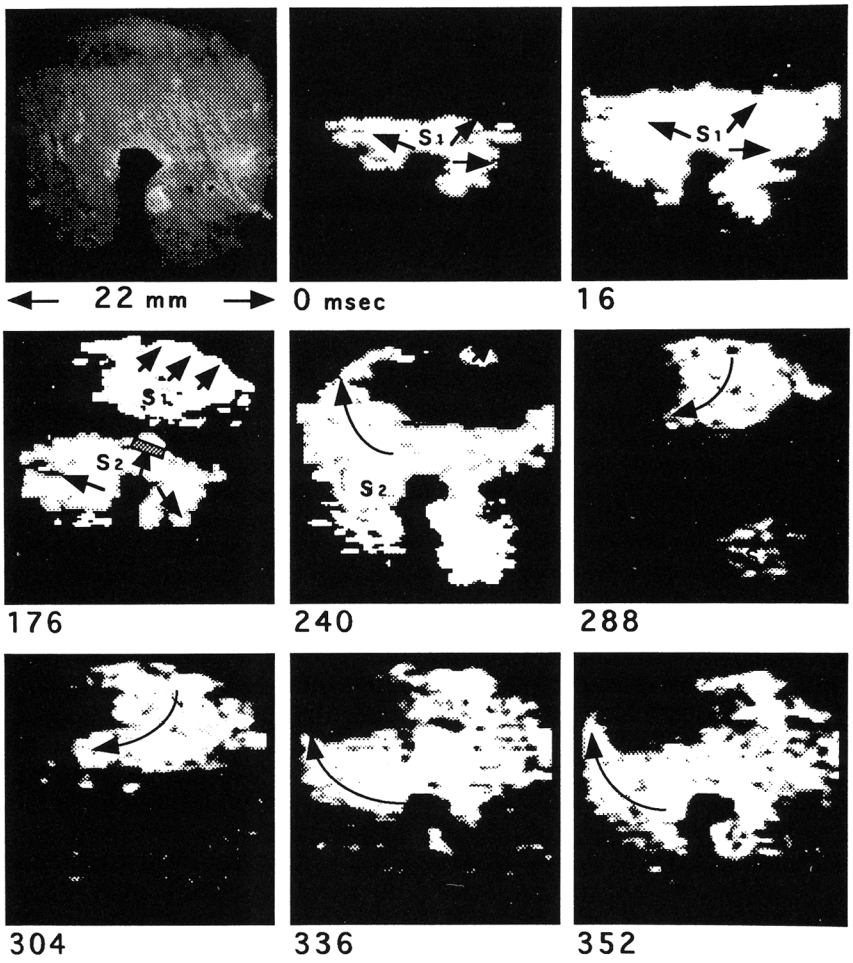

FIGURE 5. *Selected video frames obtained during spiral wave activity initiated by means of point stimulation (S_1 and S_2) in sheep epicardial muscle. The uppermost left frame shows the real image of the preparation. Note that the shadow created by the stimulating electrode runs from the center to the bottom border, thus obstructing the visualization of both the preparation and the electrical signal underneath. To improve visualization in subsequent frames, the background image of the preparation during quiescence was digitally subtracted from all the frames. Numbers at the bottom of each frame indicate time in milliseconds from an arbitrary zero time. Arrows indicate the direction of propagation of the wave front and the wave tail (at times of 176 and 240 msec). Dashed bar at 176 msec indicates propagation block. For details see the text.*

In Figure 8B we illustrate the morphology of the core and the action potential recordings revealed by the 10×10 photodiode array. Although the spatial resolution of the photodiode array recordings is less than that of the video images, the relatively high signal-to-noise ratio and time resolution of the photodiodes allowed for a more accurate analysis of the core's shape and voltage distribution at low cutoff levels. In this presentation, the geographical distribution of the fluorescence is plotted at a given cutoff level (at 20%, 30%, and 40% of the maximum fluorescence value). If one selects a cutoff level of 30%, then the core appears in this experiment as an elongated domain of 8.3×3.8 mm. Recordings from individual selected photodiodes presented at the right of panel B show that in the periphery (e.g., tracings a and e) the activity was manifested as periodic signals (T_s, 135 msec) of large amplitude, which resembled typical transmembrane potentials of cardiac muscle with rapid upstroke and slow recovery phases. In contrast, at the center (tracing c), the activity had very low amplitude.

As determined from 14 episodes analyzed, spiral wave activity in thin slices of epicardial ventricular muscle of two different species occurs around an elliptical core whose major and minor hemiaxes are 3.1±0.8 and 5.5±1.5 mm, respectively, which corresponds well with the structural properties of these tissues. Nevertheless, the ventricular site from which the epicardial tissue was obtained probably influenced the degree in fiber tortuosity from one preparation to another and gave rise to variations in the dimensions of the hemiaxes of the core.

Nonstationary Spirals

Computer simulations. The computer simulations presented above were all conducted in uniform two-dimensional matrices; i.e., within a given matrix, the properties of all cells were identical, which gave rise to stationary spiral wave activity. On the other hand, according to the theory of excitable media, the presence of parameter gradients across the matrix, however small, should result in nonstationary spirals.[36,37] The results illustrated in Figure 9 were obtained from a computer simulation (AR=3) in which the excitation threshold of the cells was modified such that the propagation velocity in the upper region of the array was normal and decreased gradually toward the bottom region. For that purpose, the following term was added to the right side of Equation 1, which is dependent on the space variable y: $\alpha(y-y_0)$, where $\alpha=0.0123$ and $y_0=5.85$. This is evidenced in panel A by the distorted front of the "planar" wave initiated by simultaneous stimulation of the entire left border of the array. As a result of the gradient, subsequent cross-field stimulation gave rise to a nonstationary spiral whose center of rotation drifted gradually downward and to the left (panels B and C) following the trajectory depicted by the dots (numbers indicate the cycle number).

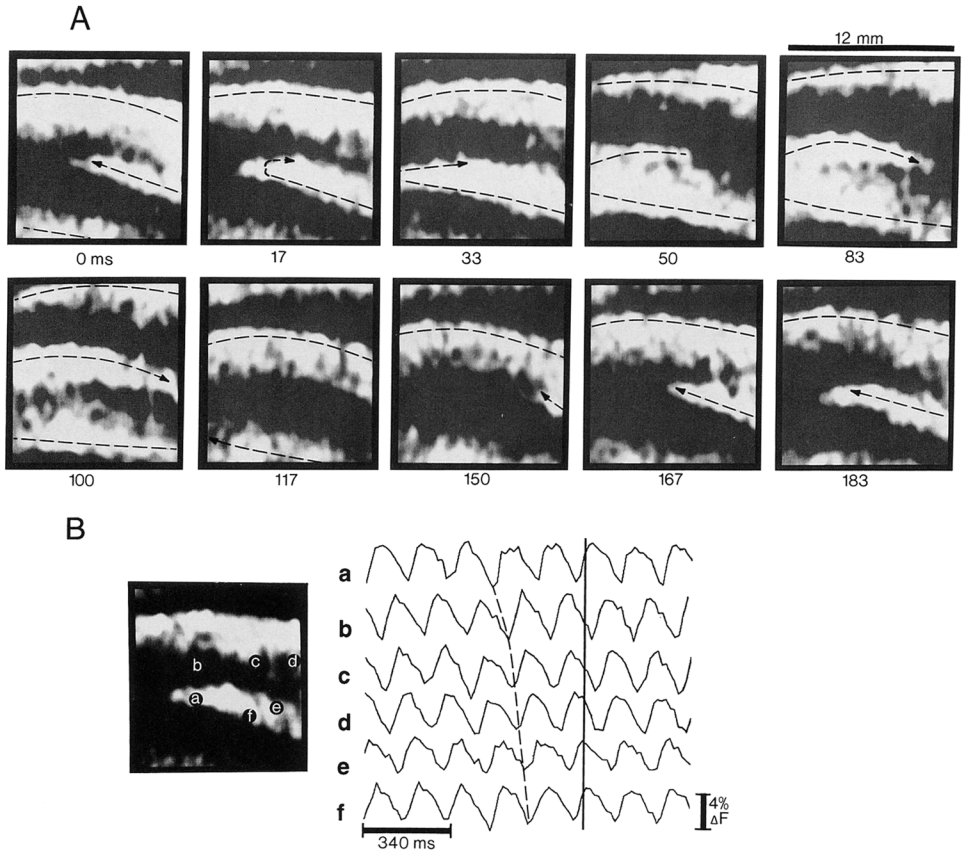

FIGURE 6. *Optical mapping of a clockwise rotating spiral wave in sheep epicardial muscle. Fibers run horizontally. Panel A: Snapshots obtained during one complete rotation. Arrows indicate the direction of propagation at the tip of the spiral. Numbers indicate time in milliseconds. The gray scale represents transmembrane voltage, with white being depolarization and black being resting potential. Panel B: Snapshot during the same episode shown in panel A (left) and time course of optical signals at the points indicated in the snapshot (right). The letters a–f indicate the location of the points selected for the recording of the action potentials; the dashed line indicates the sequence of activation; and the solid line indicates the moment at which the snapshot on the left was obtained. ΔF, relative in fluorescence.*

In Figure 9, tracings from two different individual pixels (*a and *b) located in the path of the drifting spiral are shown in panels D and E. Initially, the center of the core region was somewhat distant (see point 1 in panel B) from either of the two recording sites; action potentials were relatively normal, and almost full repolarization was achieved in both during beat 1. As the core drifted toward the two recording sites (see beats 2–5), both maximum diastolic potential (MDP) and action potential amplitude (APA) gradually declined.

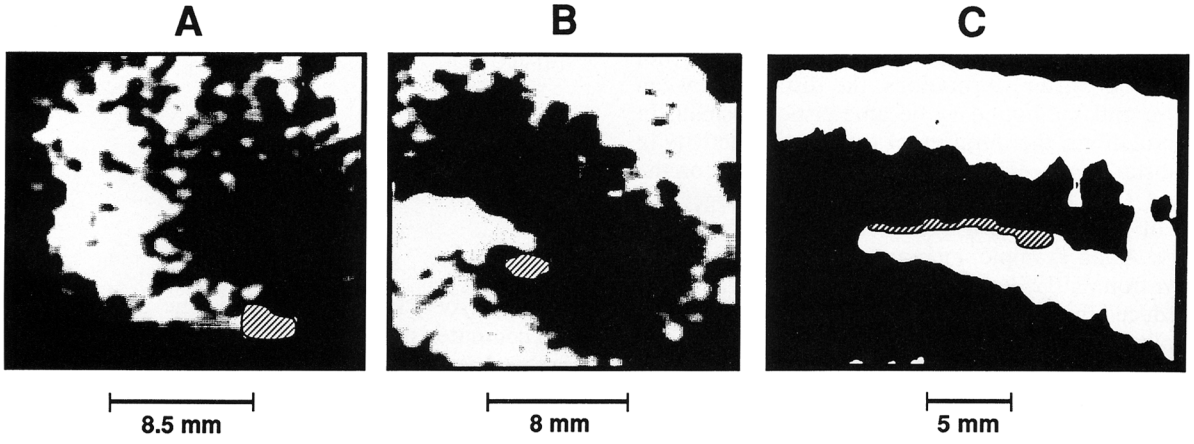

FIGURE 7. *Video images showing spiral wave activity obtained in three sheep epicardial muscle preparations with different degrees of anisotropy. All panels were oriented such that fibers run horizontally. In each panel, the dashed area represents the core as measured by means of time–space plots. Panel A: Anisotropic ratio (AR)=1.57. Panel B: AR=2.7. Panel C: AR=6.*

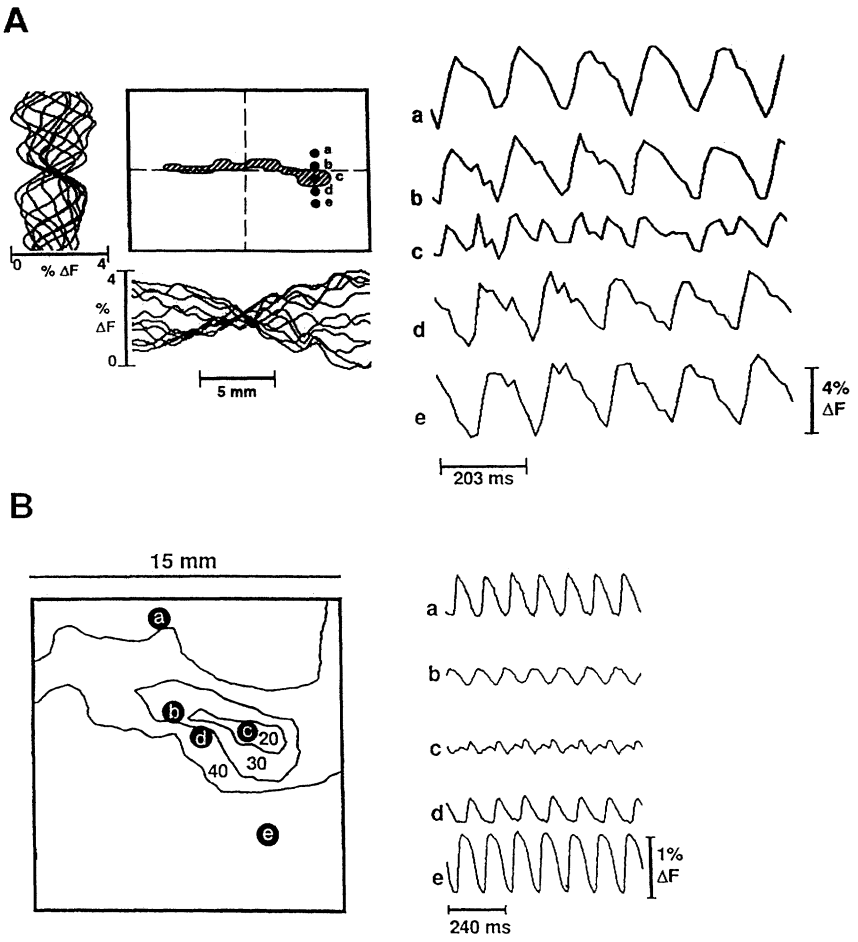

FIGURE 8. *Activity and voltage structure of the core area obtained from sheep epicardial muscle preparations. Panel A: Position of the core of the spiral wave (left) shown in panel C of Figure 7 and optical signals (right) from the points indicated at the left. The letters a–e are points across the core selected for the recording of action potentials. Profiles of voltage amplitude were obtained from the horizontal (bottom) and vertical (left) lines crossing the core center during one complete rotation at 16-msec intervals. Panel B: Isopotential regions during spiral wave activity as recorded by means of a 10×10 photodiode array (left) and optical action potentials (right) from the points indicated at the left. Numbers indicate the maximum amplitude expressed as a percentage of the absolute maximum amplitude recorded at the periphery of the preparation. The letters a–e are points at different positions around and within the core selected for the recording of action potentials. ΔF, relative in fluorescence.*

During beat 6, the center of the core had moved away from point *a (panel D), as shown by the slightly increased MDP and APA. However, at this time (beat 6), the very center of the core was located exactly at point *b, as demonstrated by the lack of dynamic membrane potential response and by the steady MDP at approximately 30% of maximum depolarization (panel E). Thereafter, as the core drifted further downward and to the left during subsequent beats, both MDP and APA recovered their nominal values, demonstrating that the two sites were normally excitable.

As the core shifted, it gradually approached the lower boundary of the matrix. Spiral wave activity ended (not shown) when, after 19 rotations, the distance between the core and the boundary became critically small. In our simulations, the duration of the rotating activity in the nonstationary regime was strongly dependent on the gradient (α). The larger the gradient, the larger the speed of the drift and the shorter the duration of the activity. As an example, increasing the excitability gradient α from 0.0123 to 0.0138 increased the drift speed and reduced the total number of rotations from 21 to 10.

Finally, it should be noted that the horizontal (perpendicular to the parameter gradient) projection of the drift velocity depends on the direction of spiral rotation. A spiral wave with a counterclockwise direction of rotation (i.e., opposite to that shown in Figure 9) initiated at the same point would drift down and to the right.

Time versus space plots. A "frame-stack" display technique was devised in an effort to simplify the analysis of the dynamics associated with drifting spiral wave activity. In each case, analysis of just two projections (horizontal and vertical) of the frame-stack display enabled us to measure the trajectory, drift velocity, and size of the core, as well as the changes in wave propagation velocity and duration of the excited state. In this manner, cumbersome and time-consuming frame by frame analysis of the recordings was avoided.

The mathematical definition of the horizontal, E(x,t), and vertical, E(y,t), frame-stack projections is as follows:

$$E(x,t)=\frac{1}{a}\int_0^a E(x,y,t)dy$$

$$E(y,t)=\frac{1}{b}\int_0^b E(x,y,t)dx$$

where E(x,y,t) is the transmembrane potential (U) in the computer simulations or the fluorescence signal (F) in the optical mapping experiments, and a times b is the frame size. The frame-stack plot displays several periods of rotation on a single picture in which the array elements or pixel values of each time step are compressed into one row (horizontal display) or column (vertical display) and then swept in time to obtain a

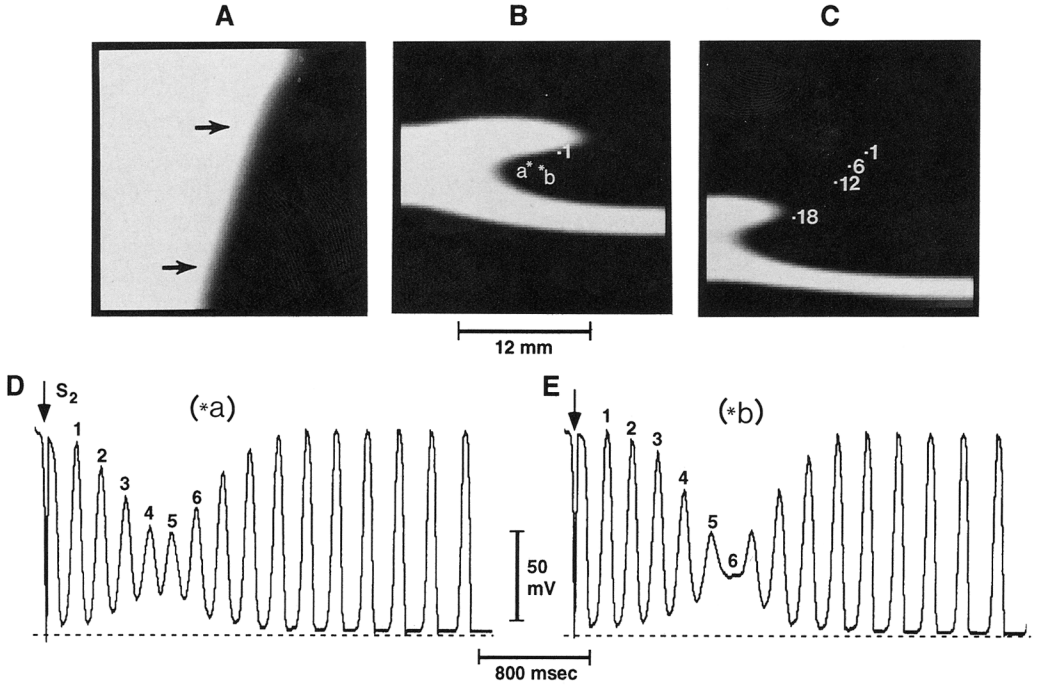

FIGURE 9. *Drifting spiral wave: numerical results. Propagation velocity decreased gradually toward the bottom region. Panel A: Snapshot of propagating wave front initiated from the left. Arrows indicate the direction of propagation. Panel B: Snapshot obtained during the first rotation of the spiral. Dot 1 indicates the instantaneous position of the core. Asterisks a and b show the sites from which action potentials (see panels D and E below) were recorded. Panel C: Snapshot obtained during the last rotation. Dots indicate the position of the core at previous cycles. Numbers indicate the cycle number. Panels D and E: Action potential changes over time from points a and b (see panel B), respectively.*

two-dimensional presentation of the activity by stacking all "frame lines" (see Figure 10).

The diagrams of Figure 10A illustrate the construction of a frame-stack display for propagation of a planar wave. The white bands of squares represent the activity propagating from left to right at a speed that is the inverse of the slope of the band. The thickness of each excitation band gives a measure of the duration of the excited state, and the vertical distance between excitation bands measures the cycle length.

Frame-stack displays for spiral waves are shown in panels B and C of Figure 10. In the presence of a rotating spiral (panel B, obtained from the same simulation as in Figure 1), there appear specific branches of relatively low amplitude in the center of the plot that occur twice every rotation period. The horizontal length of such branching bands determines the size of the core for that particular projection (i.e., either horizontal or vertical). In this simulation, the position and size of the core remained unchanged, and T_s, duration of excited state, and propagation velocity were also the same throughout. The time–space plot (horizontal projection) in panel C illustrates the case of the nonstationary spiral obtained from the simulation shown in Figure 9, which is manifested by a time-dependent shift of the core toward the left forced by the parameter gradient. Note that the size of the core increased gradually, and the rotation period (cycle length) also increased.

Frame-stack displays are especially useful for the analysis of the experimental data. Spatial averaging along one of the coordinates increases the signal-to-noise ratio and improves the accuracy in the detection of the core location.

Experimental results.

DRIFTING. Drifting spiral waves were observed in eight episodes of five experiments. The results obtained were qualitatively the same as those predicted by the computer simulations: the core drifted gradually following a predictable and steady course, with the horizontal projection of drift velocity being opposite for clockwise versus counterclockwise rotations. Results from an experiment in which spirals of opposite rotation were induced sequentially by cross-field stimulation are shown in Figure 11, panels A–D. The counterclockwise rotating spiral (panel A) drifted to the left (panel C) at a speed of 20 mm/sec, which is approximately 10% of the speed of propagation of the wave front in the direction of the drift. The clockwise rotating spiral (panel B) initiated in the same tissue a few seconds later drifted in the opposite direction and terminated at the bottom border after five cycles (panel D).

A microelectrode recording obtained during spiral wave drift is presented in panel E of Figure 11. The local dynamics of excitation and MDP are qualitatively similar to those predicted by the simulation data (see Figure 9, panels D and E). Initially, the center of the core region was somewhat distant from the recording site. Action potentials were relatively normal, and almost full repolarization was achieved during beat 1. As the core drifted toward the recording site (see beats 2–5), both MDP and APA gradually declined. During beat 6, the center of the core had moved away from the recording point, as shown by the slightly increased MDP and APA. As the core drifted away during subsequent beats, both MDP and APA recovered their nominal values, demonstrating that the core area was normally

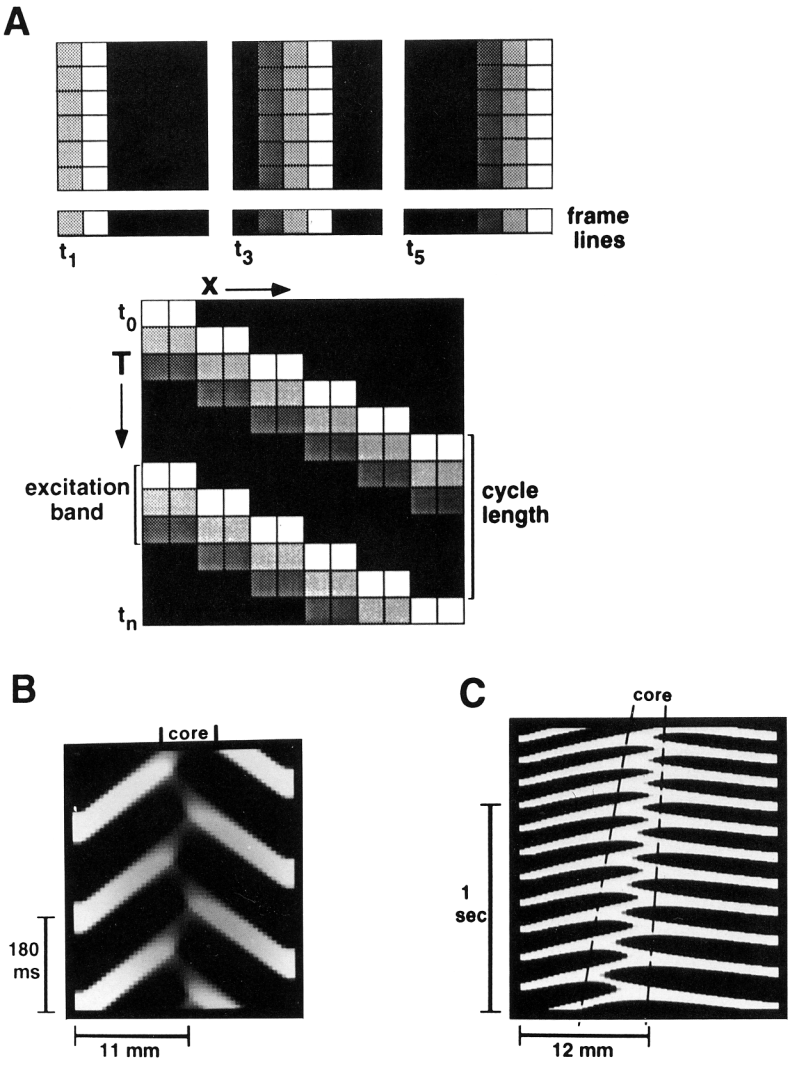

FIGURE 10. *Panel A: Construction of frame-stack plots. The top diagrams are three hypothetical video frames showing propagation of a planar wave from left to right (white, maximum depolarization; black, resting potential). The frame-stack display results from the compression of all data points of a given video frame (t_n) into a single line (represented at the bottom of each frame) and stacking all subsequent lines thus obtained (t_1, t_2 . . . t_n) onto one another to form a time–space plot (bottom diagram). Planar waves are observed as diagonal excitation bands running from left to right. The slope of the activation band is inversely related to the propagation velocity. Vertical distance (time) between two consecutive excitation bands is the cycle length; T is time; and X is horizontal distance; Panel B: Frame-stack plot obtained during stationary spiral wave in a numerical experiment. Excitation bands run from center to periphery. At the center, excitation bands are interconnected by bands of lower amplitude, which represent the activity around the core. Excitation bands are shifted in time at either side of the core. In this example, the core remained in the same position throughout the episode. Panel C: Frame-stack plot obtained during drifting spiral wave in a simulation.*

excitable. However, we should point out that, since it is very difficult to predict precisely where the core will be at a given time during the drift, we were unable to place the microelectrode in a cell within the trajectory of the core's center. However, since the changes in MDP and APA generally depend on how far the recording site is from that center (see Figure 10), we are confident that our recording was located very few cell lengths away from it.

In eight episodes, the average Vwp/Vd ratio, where Vwp is the velocity of wave propagation and Vd is the velocity of the drift, was 9.8±2.1. We were unable to find any correlation between the direction of the drift and the cell orientation.

DRIFTING AND ANCHORING. In a number of episodes, after a short period of drift, the core appeared to anchor to a small artery or other heterogeneity in the tissue, which converted the spiral wave activity into the stationary regime. When this occurred, the spiral continued to rotate around such an artery for an indefinite period of time. To our knowledge, such "anomalies" have never been described in the theoretical or experimental literature.

In Figure 12, we illustrate the phenomena of drifting and anchoring in three different episodes in the same preparation of canine epicardial muscle. The intensity of the S_2 and the S_1-S_2 interval were changed from one episode to another, which created spirals at different initial locations. In panel A (S_1-S_2=117 msec; S_2 intensity, 5 V), the core originated in the lower half of the tissue (cycle 1) and drifted toward the left (see time–space plot), first upward (cycles 2 and 3) and then downward (cycles 4 and 5), approaching the left border and terminating immediately after the fifth cycle. In panel B (S_1-S_2=110 msec; S_2 intensity, 5 V), an S_2 stimulus applied at a slightly shorter S_1-S_2 interval gave rise to rotating activity with a different drift pattern. The core, first located close to the center of the tissue (cycle 1), drifted upward and slightly to the right (cycle 2) but subsequently changed its course and moved toward the left, always approaching the upper border of the preparation. In the case of panel C (S_1-S_2=100 msec; S_2 intensity, 3.5 V), after the first cycle, the core drifted rapidly downward and toward the right, finding in its course a small artery to which it appeared to anchor. In this case, the spiral wave activity changed into the stationary regime and remained stable for more than 20 minutes.

To determine whether the anchoring phenomenon indeed results from the presence of small discontinuities

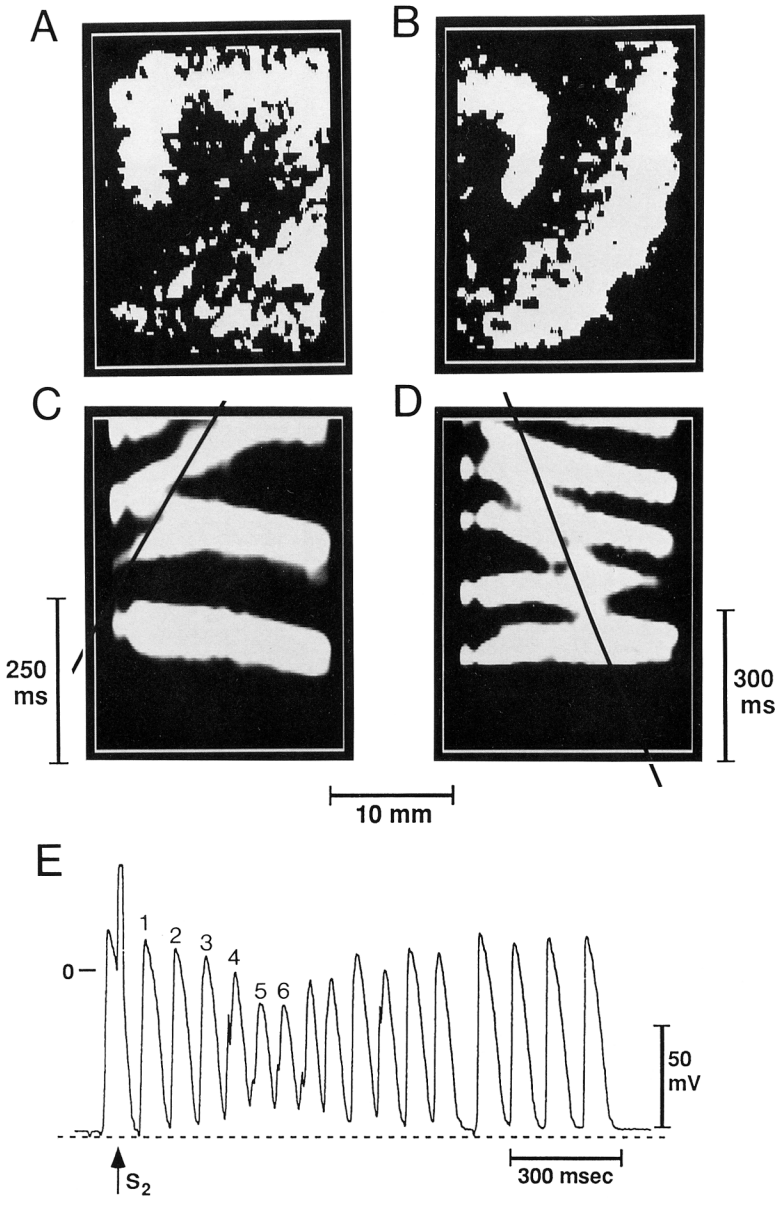

FIGURE 11. *Panels A and B: Counterclockwise and clockwise rotating spiral waves initiated in the same canine epicardial muscle preparation by cross-field stimulation. In both episodes, stimulus S_1 was applied to the left border of the tissue. Stimulus S_2 was applied either to the top (panel A) or to the bottom (panel B). Panels C and D: Frame-stack plots obtained during episodes A and B, respectively. Solid bars indicate the trajectory of the core. Direction of drift was from right to left during counterclockwise rotation and from left to right in the clockwise rotation. Panel E: Microelectrode recording obtained during the initiation of a drifting spiral wave in a different experiment. First action potential is the last response of a train of 10 basic stimuli (basic cycle length of 300 msec). After an S_2 stimulus, self-sustaining activity was initiated. The recording site was at the core region during action potentials 5 and 6.*

in the excitable medium, we carried out additional simulations in which we attempted to approximate the nonuniformities that are inherent to the cardiac muscle and might be encountered by a drifting spiral wave. Thus, in the new simulations, in addition to an excitability gradient across the array (see Figure 9), a small region was rendered inexcitable. The results are illustrated in Figure 13. When the core of the drifting spiral found the unexcitable obstacle in its path, it abruptly became attached to it, and the rotation changed from the nonstationary to the stationary regime. As the spiral drifted, the period was gradually prolonged from 192 to 240 msec (see panel B). After anchoring, the duration of the period of rotation increased to 320 msec and remained stable for the remainder of the simulation.

Additional simulations (not shown) demonstrated that anchoring occurred only when the distance between the obstacle and the tip of the travelling spiral was relatively small (i.e., <2×core radius).

The Doppler effect. As is the case for any wave source that moves in space, drifting of a spiral wave resulted in a Doppler shift in the period of excitation: the excitation period ahead of the drifting core was always shorter than that behind the core, the difference being larger for higher drift velocities. This Doppler effect is illustrated by the experimental data presented in Figure 14. The core initially appeared near the left border of the preparation and drifted at a constant velocity of approximately 6 mm/sec toward the right (see panel A). One can see that the period of excitation ahead of the moving core was approximately 40 msec (approximately 20%) shorter than excitation period behind the core. The time course of the changes in fluorescence (panel B) shows clear difference in excitation frequency between tracings a and d recorded behind the core and ahead of the core, respectively. In fact, within the same time interval, five action potentials were recorded in tracing a and six action potentials were recorded in tracing d.

The Doppler shift in the excitation period also resulted in cyclic variations in the apparent site of initial excitation. For example, during the second action po-

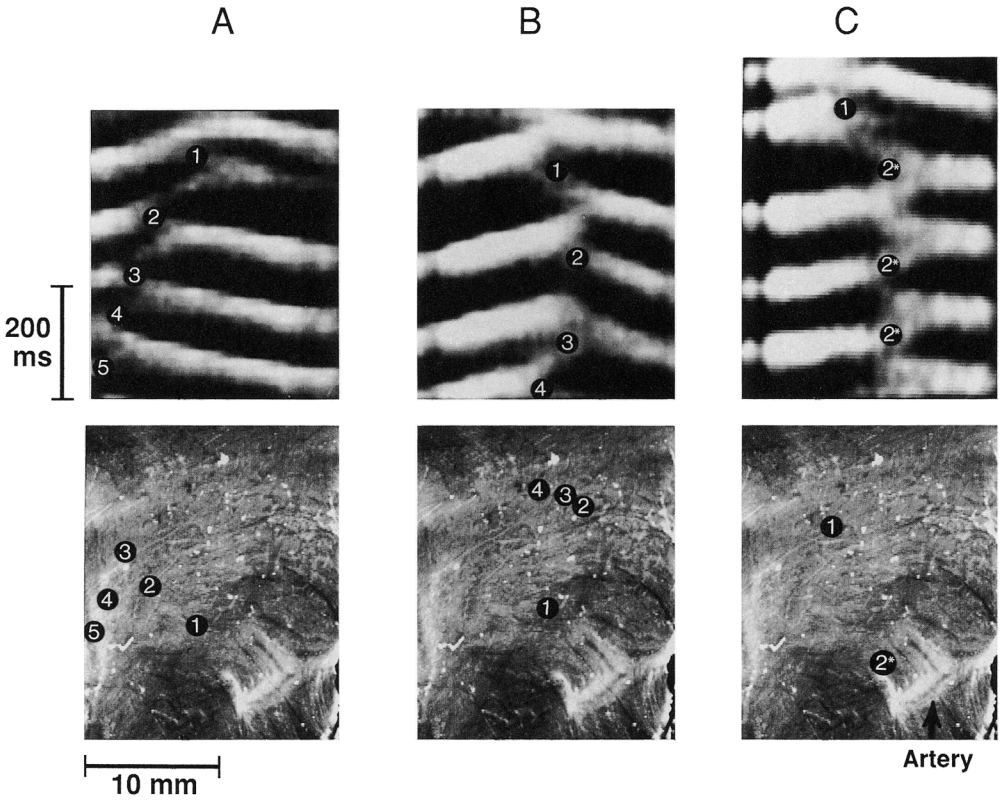

FIGURE 12. *Drifting and anchoring of spiral waves initiated in a canine epicardial muscle preparation. The arrangement of stimulating electrodes was the same in all episodes. Stimulus S_1 was delivered to the left border, and S_2 was delivered to the top border. Each panel depicts the frame-stack plot (horizontal projection) during four rotations (top) and the real image of the preparation (bottom). Black dots indicate the position of the core during different rotations; numbers indicate the rotation number. Panel A: The core drifted to the left (as shown in the frame stack) and upward during the first three rotations and then to the left and downward. Panel B: The core drifted upward and to the right and then upward and to the left. Panel C: The core drifted downward and to the right during the first rotation. After the second rotation, the core remained stationary in the same position; 2* shows the position of the anchored core during all subsequent rotations.*

tential, activation occurred first in tracing a and later in tracing d. However, during the fifth action potential, activation occurred first in tracing d and later in tracing a. Moreover, as the core drifted across points b and c, their fluorescence signals demonstrated the low voltage activity expected from recordings near the core center (see Figures 9 and 11).

Whether in the computer simulations (see Figure 10C) or the experimental results (see Figures 11C, 11D, 12A, 12B, and 14), drifting was always accompanied by a Doppler shift in the excitation period. In fact, in those cases in which the drift direction varied (see Figures 12A and 12B), the Doppler effect gave rise to complex aperiodic patterns of activation (see below).

Simulated electrocardiogram obtained during spiral wave activity. To analyze the global patterns produced by spiral wave activity, simultaneous horizontal and vertical lead recordings of a pseudoelectrocardiogram were obtained from both simulations and experiments (Figure 15). Two different examples are illustrated for each case: one for drifting and the other one for anchoring spiral wave activity. In the presence of drift spiral, there is an undulating pattern (waxing and waning), whereby the axis of the depolarization complex (i.e., the "QRS" complex) suffers a gradual torsion. The cycle length gradually decreases during 20 (in the simulation) and 13 (in the experiment) rotations before the termination of the episode. During anchoring (indicated by the asterisk), a period of irregular activity is followed by uniform and regular events in both computer and experimental tracings. In the examples shown, anchoring occurred after 10 rotations of spiral wave activity. Note that stabilization is followed by change in the morphology of the QRS complexes and prolongation of the cycle length.

Discussion

Self-sustaining rotating spiral waves can be induced in small two-dimensional pieces of cardiac muscle. Moreover, the entire course of the excitation–recovery process during the reentrant cycle can be analyzed in detail through the use of optical mapping and voltage-sensitive dyes. The results show that spiral wave activity may be induced by premature stimulation in thin slices of isolated ventricular epicardial muscle. Indeed, similar to what was shown in chemical reactions,[12,13] rotating waves in the heart have a pronounced spiral shape with curvature increasing toward the center of rotation. The organizing center of the spiral, the core, is a finite small domain of unexcited but excitable tissue that determines the main properties of the spiral: its period of rotation and the excitable gap.[12,30] As demonstrated by

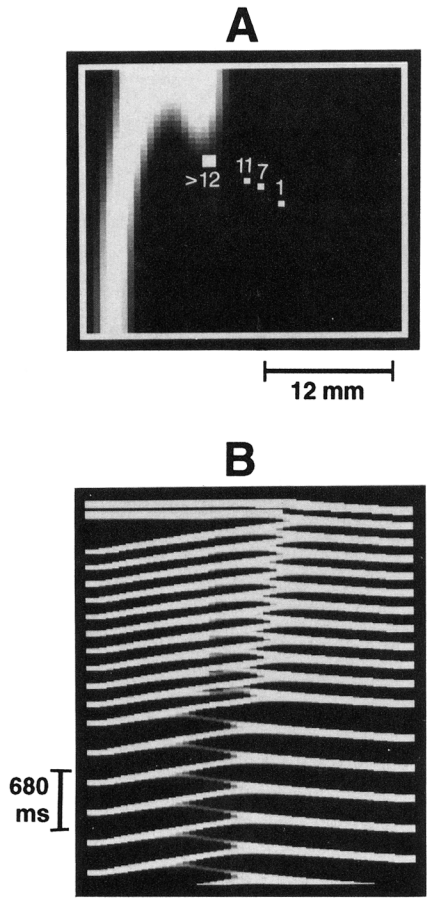

FIGURE 13. *Anchoring of spiral wave in the two-dimensional model. Four cells (large square) were rendered unexcitable by making transmembrane potential* U=*0 in those elements. The parameter gradient was the same as in Figure 9 but rotated 90°. Panel A: Snapshot of a clockwise-rotating spiral that drifted upward and to the left. White dots indicate the positions of the core during different cycles. Panel B: Frame-stack plot during the first 17 rotations of the episode shown in panel A. Anchoring occurred after the 12th rotation.*

our experiments, in the heart muscle, the core is elliptical as a result of the inherent anisotropy of the tissue. Within the core, action potentials are shown to have low amplitude and slow upstroke velocity. In addition, the core of the spiral can either be stationary or drift away from its site of origin. Finally, drifting spirals are attended by Doppler shifts of the activation frequency.

Relevance of the Computer Model

Various types of models have been used to simulate propagation of excitation in heart tissue. These range from very simple cellular automata models[38–41] to highly complex ionic models that rely on partial differential equations of the Hodgkin and Huxley type.[42,43] The model we have used in the present study is based on FHN equations,[26–31] which have an intermediate level of complexity. The FHN model is not an ionic model in the common sense, since all slow ionic currents are combined into one variable that is responsible for repolarization and recovery of excitability. Thus, as such, the model cannot be used to study ionic mechanisms responsible for the system's behavior but rather to provide analytical and qualitative representations of that system's dynamic properties.[26–31]

We have used a very simple version of FHN equations with piecewise linear approximation of all nonlinear functions.[28,29] In selecting the model parameters, we have attempted to approximate as much as possible the electrophysiological characteristics of the myocardial tissue. However, its representation of the action potential shape is less accurate than that provided, for example, by the model of van Capelle and Durrer.[27] Yet our version requires much less computational resources while at the same time providing reasonable qualitative results. We have introduced two modifications in the generic FHN model. First, we adjusted the parameters c_2 and τ_3 in such a way as to obtain the same T_s/T_r ratio as that observed in our experiments (T_s/T_r, approximately 1.4; see "Results"). Second, we introduced continuous anisotropy in the diffusion term of the equation, which closely simulated the conditions of larger longitudinal than transverse conduction velocity in normal ventricular epicardial muscle of sheep[32,34] and dog.[35] As such, the model does not account for all phenomena associated with propagation in cardiac muscle at the microscopic scale.[44] Yet, as confirmed by our experimental studies, the model is sufficient to explain many global features of spiral wave reentrant activity, including the shape of the wave front and, more importantly, the properties of the core and drift phenomenon.

Limitations of the Experimental Approach

The preparation. The electrophysiological characteristics of our preparations were measured by means of intracellular microelectrodes during basic stimulation. Transmembrane potentials were found to be normal in terms of resting membrane potential, action potential upstroke velocity, and action potential duration. Values of conduction velocity for longitudinal (CV_L) and transverse (CV_T) propagation (0.39±0.14 and 0.14±0.07 m/sec, respectively) were very close to those reported recently in studies in which a similar preparation was used (CV_L=0.34±0.03 m/sec; CV_T=0.11±0.01 m/sec).[32] In addition, such values compare well with those obtained in slices of canine epicardial muscle (CV_L=0.43 m/sec; CV_T=0.2 m/sec),[45] calf endocardial trabeculae (CV_L=0.48 m/sec; CV_T=0.16 m/sec),[46] and whole-heart preparations in which conduction velocities were measured on the surface of the epicardium (CV_L=0.7 m/sec; CV_T=0.08 m/sec).[47]

Our experiments demonstrate stationary as well as drifting spiral wave activity in cardiac muscle. However, extreme caution should be exerted to prevent direct extrapolation of our results to the whole heart or to the clinical situation. The experiments were carried out in very thin pieces of ventricular epicardial muscle, which were cut in such a way as to confine the propagation of electrical waves to two-dimensional space. Thus, one cannot draw any final conclusions about whether our results may or may not relate to arrhythmic behavior in the heart. Nevertheless, it is tempting to speculate that perhaps some relation exists between the two-dimensional spirals documented in this study and the reentrant tachycardias recorded in experimental models of transmural infarction of the left ventricular wall in which a thin rim of viable epicardial muscle remains.[23] Confirmation of such a relation, however, awaits the

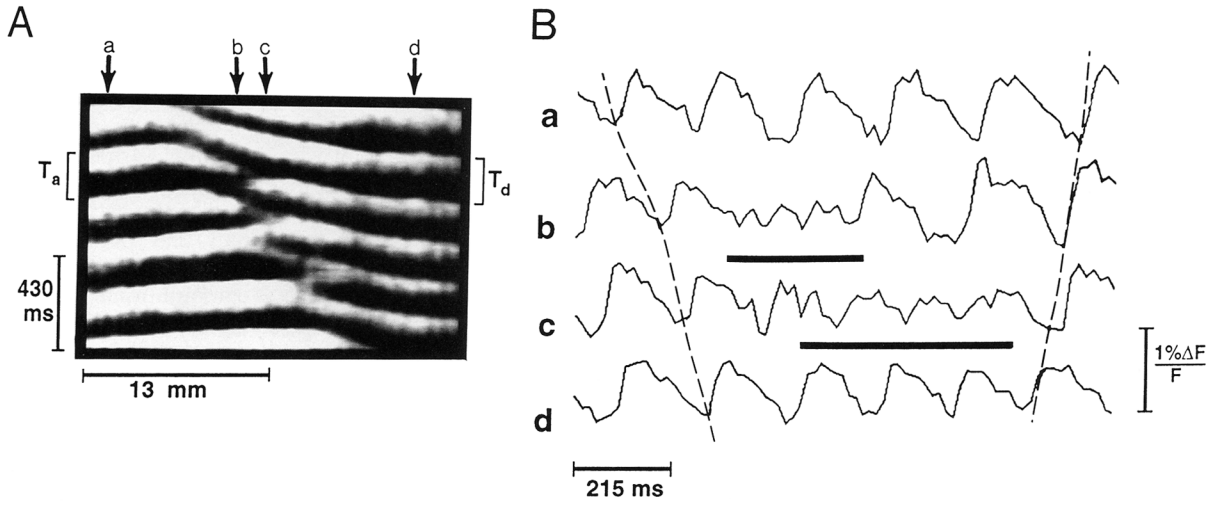

FIGURE 14. *Doppler effect of drifting spiral wave activity in sheep epicardial muscle. Panel A: Frame-stack display. The core drifted from left to right. T_a and T_d indicate rotation periods in the region that are behind and ahead of the core, respectively; the letters a–d indicate the horizontal position of the recordings shown on the right panel. Panel B: Optical action potentials recorded from points that are behind and ahead of the core (tracings a and d, respectively) and from points that are first ahead and then behind the core (tracings b and c). Diagonal lines indicate the approximate activation sequence during the second and last rotations. Horizontal bars indicate irregular low voltage activity recorded in points b and c as they were visited by the core early and late, respectively, during the episode. ΔF/F, relative change in fluorescence.*

development of new experimental approaches using high-resolution mapping of heart surface.

The optical mapping setup. The system has some important limitations that should be considered. First, the time resolution of the video camera is only 60 frames per second or 16.7 msec of frame-to-frame interval. This precludes any quantitative analysis of rapid events, such as action potential upstroke and local changes in conduction velocity, at the microscopic scale. Second, the signal-to-noise ratio is low, only approximately 1:1 before filtering, which is much inferior to the ratio of 30:1 achieved with the photodiode array. To improve the signal-to-noise ratio of our video recordings, we applied a spatial convolution filter with a cone-shaped kernel of 15 pixels in diameter, which corresponded to an effective spatial resolution of 0.4–0.5 mm. This is a low-pass filter that eliminates high spatial frequencies such as step edges or highly curved structures, thus flattening small curvings of the wave front. This limitation of the video camera is not critical for the analysis of global features of spiral waves (such as drift and anchoring). In fact, for the detailed analysis of the voltage structure of the spiral wave and its core, we used a combination of the techniques of photodiode and video camera recordings plus single microelectrodes.

Finally, one of the major technical drawbacks in recording optically from heart tissue is the mechanical artifact produced by the contraction. Investigators have attempted to overcome this limitation by sandwiching the heart between two glass windows and pressing Lucite pads against the two other sides of the heart.[48] In other investigations, preparations were superfused with calcium-free solutions.[49] In our experiments, we have elected to superfuse the preparations with Tyrode's solution containing DAM, which totally suppresses contractility but produces only small alterations in the electrical activity.[50,51] In fact, a recent study has shown that 15 mM DAM produces a small decrease in action potential duration but does not significantly affect upstroke velocity or amplitude (Y. Liu, personal communication). Action potential duration decreases by approximately 20% at a BCL of 300 msec, but the decrease is less at cycle lengths between 100 and 250 msec, which is typically the range of periods of the sustained tachycardias demonstrated in our experiments. Such effects on the action potential are well correlated with a drug-induced 10–20% decrease in the L-type inward calcium current, as demonstrated by recent patch-clamp experiments in single guinea pig ventricular myocytes[51] (also, Y. Liu, personal communication). Nevertheless, to ensure that DAM was not affecting our ability to initiate or sustain the rotating activity, repetitive activity was induced in most of the experiments by cross-field or point stimulation before (recorded with microelectrodes) and after (optical mapping) superfusion with DAM.

Concepts of Curvature and Singularity

An important issue that has not been contemplated in traditional concepts of functional reentrant excitation is that the propagation velocity of a wave front is very much dependent on its curvature; convex wave fronts must excite more tissue than concave wave fronts; therefore, they propagate at slower velocities. It follows that since different segments of a spiral wave have different curvatures, they should have different conduction velocities. Moreover, analytical studies of stationary spiral waves show that, within a given parameter range, the core is comprised of fully excitable tissue, yet the tissue in its center is never excited as a result of the extremely pronounced curvature at the tip of the rotating wave front.[28,30]

A major contribution of the theory of spiral waves that has only recently found its way into cardiac electrophysiology in Western literature is the concept of "singularity".[9,30,52] As illustrated diagrammatically in

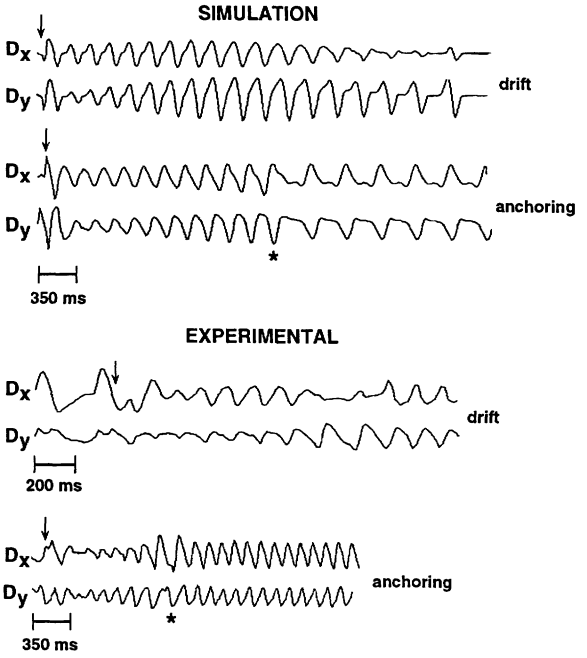

FIGURE 15. *Pseudoelectrocardiogram obtained during drifting and anchoring spiral wave activity in computer simulations and experimental preparations. In each example, D_x and D_y are the horizontal and vertical leads, respectively, calculated as described in "Materials and Methods." Arrows indicate the occurrence of the S_2 stimulus. The asterisk represents the moment of anchoring. Top panel: The top two tracings are the horizontal and vertical leads obtained in a computer simulation during the episode of drifting spiral wave shown in Figure 9. The D_x lead shows a clear undulating "QRS" pattern while the spiral is progressively moving from right to left and top to bottom; the lower two tracings are the horizontal and vertical leads obtained from the episode of anchoring of spiral wave shown in Figure 13. Irregular activity is followed by regular activity. Note the change both in rate and morphology of the QRS complexes after anchoring. Bottom panel: The top two tracings are the horizontal and vertical leads obtained during drifting spiral wave activity from optical mapping experiments. In both leads, undulating patterns of the QRS complexes are observed. The lower two tracings are the horizontal and vertical leads obtained during anchoring of the spiral wave. Similar to the results obtained in computer simulation, an episode of irregular activity was followed by activity with a uniform QRS pattern.*

Figure 16, during propagation initiated by a linear source (i.e., a planar wave; panel A) or by a point source (i.e., a circular wave; panel B), the wave front is always followed by a recovery tail of finite dimensions. In other words, the front and the tail never meet each other anywhere,[30] and the local distance between the front and the tail at any segment of the wave corresponds to the so-called "wavelength" of excitation at that particular segment. In contrast, when spiral wave propagation is initiated, a unique phenomenon takes place, whereby the wave front and wave tail actually touch each other at a specific point of singularity[30,52] (q point, panel C), which corresponds to the site where a wave break has occurred (see Figure 1) and where propagation of the wave front is extremely slow. Indeed, breaking of a propagating wave as a result of collision with the refractory tail of another wave leads to curling and initiation of the spiral wave activity (see Figure 1). Thus the q point acts effectively as the pivoting point that forces the wave to rotate around the core of unexcited but excitable tissue.[30]

Curvature, Anisotropy, and the Excitable Gap

In contrast to the long-held view that anisotropy is responsible for the presence of an excitable gap between the head and the tail of functional reentry in ventricular myocardium,[23,24] our computer simulations show that neither the period of rotation nor the refractory period changes when the anisotropic ratio is increased by as much as four times. The only effect of anisotropy is that of changing the shape of the spiral from circular to elliptical. From the topological point of view, an ellipse may be transformed into a circle, thus, the equations for isotropic excitable media may be easily converted into anisotropic by simply scaling the space variables of the system.[53]

More importantly, slowly rotating spirals with a wide excitable gap are demonstrable even in totally homogeneous isotropic excitable media. In such cases, the necessary condition for the presence of an excitable gap is in fact the presence of a very steep positive curvature near the tip of the spiral wave front. As a result of such a curvature, both the local current density and safety factor for excitation of tissue ahead of the tip are greatly reduced; thus, the conduction velocity of the impulse is also reduced. This means that very slow rotation is possible even in the presence of a fully excitable gap. These theoretical concepts are still awaiting experimental confirmation. It should be pointed out, however, that the presence of discontinuities in our preparations may also have contributed to the formation of an excitable gap.

Drifting and Anchoring of Spiral Waves

A useful contribution of the concept of spiral wave reentry to experimental cardiology is the demonstration of the drift phenomenon. Movement and changes in shape of the "arc of conduction block" have been described in the experimental literature,[3,54] but with very few exceptions,[7,55] the importance of that phenomenon and its mechanism were not recognized or studied. Yet, it seems clear that drifting implies short circuiting of the wave front through the core of the spiral, which is compelling evidence that the core is indeed composed of excitable nonrefractory tissue.

According to the theory of excitable media, drift may be a result of spatial gradients in such parameters as refractory period,[55] fiber orientation, and excitation threshold[36,37] or may appear in bounded excitable media as a consequence of interaction of the core with the border of the medium.[56] In the latter case, the spiral wave may drift along the boundary at a distance that is close to the critical radius (i.e., the minimum radius of that region that is necessary to maintain a spreading wave). We did not attempt to determine systematically in our experiments whether parameter gradients were indeed present in the preparations under study. However, healthy myocardial tissue is well known to have nonuniformities in refractoriness, excitability, and fiber

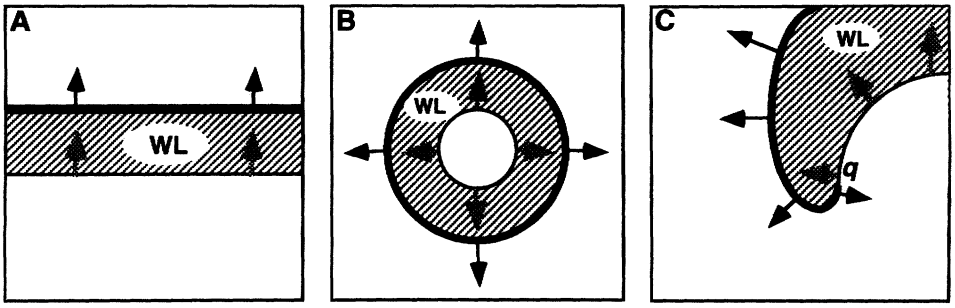

FIGURE 16. *Schematic representation of propagating waves in a homogeneous isotropic medium. In each panel, the thick black edge represents the wave front, and the dashed area represents the repolarizing tail. Black arrows indicate the direction of propagation of the wave front, and dashed arrows indicate the direction of the wave tail. The distance between the wave front and tail of repolarization is the wavelength (WL). Panel A: Planar wave initiated by stimulation of the entire bottom border of the array. Panel B: Circular wave initiated by stimulation of a point in the center of the array. Panel C: Spiral wave. The wave front has variable curvature and conduction velocity (length of arrow indicates relative conduction velocity). Note that there is a point (q) where the wave front fuses with its own repolarizing tail.*

orientation, which makes it an ideal substrate for spiral wave drift. Our study provided strong evidence for such a drift in isolated heart tissue slices. As measured by time–space plots, drift velocity could be as high as 30 mm/sec, which is approximately 10% of normal speed of activation in the same direction.

Multiple mechanisms may cause the drift, which makes it very difficult at the present time to distinguish which one is responsible for the phenomenon in any particular episode. This issue requires further detailed investigation and careful measurements of parameter gradients. Analysis of our experimental results shows, however, that interaction with the borders plays a negligible role in the mechanism of drift. Indeed, in six of seven experiments, the distance between the core and the border was not constant, and there was no correlation between the border-to-core distance and the drift velocity.

In general, drifting spirals are relatively short-lived. In our experiments, drifting spirals either terminated spontaneously after a few rotations or became stationary by anchoring to small discontinuities represented by localized regions of poor excitability. A very similar anchoring phenomenon has been observed recently in the Belousov-Zhabotinsky reaction, in which a small unexcitable area was created by pointing a laser beam into the medium (S. Müller, personal communication).

Drift Phenomenon and Possible Implications

The "spiral wave" concept provides new insight into the mechanism of spontaneous termination of nonsustained tachycardias. Collision of the core of a drifting spiral wave with the border of the excitable medium results in the collapse of the rotating wave.[56] In all (n=8) documented episodes of short-lasting tachycardia in our sheep and dog preparations, collision of the core with the tissue border was indeed responsible for the termination of the tachycardia. According to theory, the velocity of the drift is highly dependent on the size of the parameter gradient; the larger the gradient, the faster the drift and, by inference, the shorter the duration of the spiral wave episode. Application of these concepts to the study of ventricular tachycardias should provide new avenues for research in the understanding, treatment, and prevention of nonsustained tachycardias.

The drift phenomenon is accompanied by a Doppler effect and results in activation patterns that resemble those recorded in patients with polymorphic ventricular tachycardia of the type known as torsade de pointes.[57] Since the original description of torsade de pointes by Dessertenne,[58] the periodic torsion of the QRS axis was attributed to the presence of two widely separated automatic foci firing at slightly different frequencies. In fact, although other mechanisms have been proposed,[59–61] electrical stimulation of the ventricles from two points with slightly different frequencies was demonstrated to result in electrocardiographic patterns similar to those described in cases of torsade de pointes.[62] One of the problems of the "two-foci" hypothesis is that it requires simultaneous initiation and termination of both foci in each episode of tachycardia. Our postulate, which is also based on the existence of two coexisting frequencies, suggests that those frequencies may be originated from a single source, a moving spiral wave. Moreover, the observation that drifting is accompanied by a Doppler effect supports the hypothesis that a drifting spiral (i.e., a single source) occurring in the heart may produce a twisting pattern in the axis of the QRS complexes. However, since our preparations consist of two-dimensional cardiac tissue with an unrealistic boundary condition (i.e., isolated tissue), the simulated electrocardiogram may not be equivalent to a real electrocardiogram obtained from the entire heart. Accordingly, this hypothesis remains to be tested in the heart in situ.

Conclusion

We have shown in this study that theoretical predictions derived from the analysis of generic excitable media have a bearing on the mechanisms and dynamics of normal cardiac excitability and reentry. Much of the abnormal function studied in heterogeneously damaged myocardial tissue, and commonly attributed to variable and complex abnormalities, may also be demonstrated in normal tissue and is in fact demonstrable in any kind of excitable medium. Hence, one of the most important conclusions from our results is that it is possible to combine dynamic systems theory together with an elec-

trophysiological description of normal myocardium to understand abnormal function. We are not the first who have proposed such an approach (see References 8 and 9), but hopefully we have provided some new strong arguments in its favor.

Acknowledgments

We thank Dr. John Kauer and Dr. Gino Cinelli for their invaluable assistance in developing our video optical mapping system and Dr. Leslie Loew for providing the dyes. We also thank Dr. Donald Michaels and Dr. Mario Delmar for reading the manuscript, Professor Arthur T. Winfree for helpful suggestions, and Wanda Coombs, JoAnne Getchonis, and Chris Kapuscinski for their technical assistance.

References

1. Wellens HJJ, Durrer DR: Observations on mechanisms of ventricular tachycardia in man. *Circulation* 1976;54:237–246
2. Horowitz LN, Josephson ME, Harken AH: Epicardial and endocardial activation during sustained ventricular tachycardia in man. *Circulation* 1980;61:1227–1238
3. Frazier DW, Wolf PD, Wharton JM, Tabg ASL, Smith WM, Ideker RE: Stimulus-induced critical point: Mechanism for the electrical initiation of reentry in normal canine myocardium. *J Clin Invest* 1989;83:1039–1052
4. Davidenko JM, Kent P, Chialvo DR, Michaels DC, Jalife J: Sustained vortex-like waves in normal isolated ventricular muscle. *Proc Natl Acad Sci U S A* 1990;87:8785–8789
5. Jalife J, Davidenko JM, Michaels DC: A new perspective in the mechanisms of arrhythmias and sudden cardiac death: Spiral waves of excitation in heart muscle. *J Cardiovasc Electrophysiol* 1991;2: S133–S152
6. Davidenko JM, Kent P, Jalife J: Spiral waves in normal isolated ventricular muscle. *Physica D* 1991;49:182–197
7. Davidenko JM, Pertsov AM, Salomonsz R, Baxter W, Jalife J: Stationary and drifting spiral waves of excitation in isolated cardiac muscle. *Nature* 1991;355:349–351
8. Krinsky VI: Mathematical models of cardiac arrhythmias (spiral waves). *Pharmacol Ther* 1978;3(pt B):539–555
9. Winfree AT: Electrical instability in cardiac muscle: Phase singularities and rotors. *J Theor Biol* 1989;138:353–405
10. Tyson JJ, Keener JP: Spiral waves in a model of myocardium. *Physica D* 1987;29:215–222
11. Krinsky VI, Biktashev VN, Pertsov AM: Autowave approaches to cessation of reentrant arrhythmias. *Ann N Y Acad Sci* 1990;591: 232–247
12. Winfree AT: Spiral waves of chemical activity. *Science* 1972;175: 634–636
13. Muller SC, Plesser T, Hess B: The structure of the core of the spiral wave in the Belousov-Zhabotinsky reagent. *Science* 1985;230: 661–663
14. Gerisch G: Standienpezifische Aggregationsmuster bei Distyostelium Discoideum. *Wilhelm Roux Archiv Entwick Org* 1965;156: 127–144
15. Gorelova NA, Bures J: Spiral waves of spreading depression in the isolated chicken retina. *Neurobiology* 1983;14:353–363
16. Lechleiter J, Girard S, Peralta E, Clapham D: Spiral calcium wave propagation and annihilation in *Xenopus laevis* oocytes. *Science* 1991;252:123–126
17. Mines GR: On circulating excitation on heart muscles and their possible relation to tachycardia and fibrillation. *Trans R Soc Can* 1914;4:43–53
18. Garrey WE: Auricular fibrillation. *Physiol Rev* 1924;4:215–250
19. Lewis T: *The Mechanism and Graphic Registration of the Heart Beat.* London, Shaw, 1925
20. Allessie MA, Bonke FIM, Schopman FJC: Circus movement in rabbit atrial muscle as a mechanism of tachycardia. *Circ Res* 1973; 33:54–62
21. Allessie MA, Bonke FIM, Schopman FJC: Circus movement in rabbit atrial muscle as a mechanism of tachycardia: II. The role of nonuniform recovery of excitability in the occurrence of unidirectional block as studied with multiple microelectrodes. *Circ Res* 1976;39:168–177
22. Allessie MA, Bonke FIM, Schopman FJC: Circus movement in rabbit atrial muscle as a mechanism of tachycardia: III. The "leading circle" concept: A new model of circus movement in cardiac tissue without the involvement of an anatomical obstacle. *Circ Res* 1977;41:9–18
23. Dillon SM, Allessie MA, Ursell PC, Wit AL: Influence of anisotropic tissue structure on reentrant circuit in the epicardial border zone of subacute canine infarcts. *Circ Res* 1988;63:182–206
24. Wit AL, Dillon SM, Coromilas J, Saltman AE, Waldecker B: Anisotropic reentry in the epicardial border zone of myocardial infarcts. *Ann N Y Acad Sci* 1990;591:86–108
25. Beeler GW, Reuter H: Reconstruction of the action potential of myocardial fibres. *J Physiol* (Lond) 1977;268:177–210
26. FitzHugh RA: Impulses and physiological states in theoretical models of nerve membrane. *Biophys J* 1961;1:445–466
27. van Capelle FJ, Durrer D: Computer simulation of arrhythmias in a network of coupled excitable elements. *Circ Res* 1980;47:454–466
28. Pertsov AM, Emarkova EA, Panfilov AV: Rotating spiral waves in modified FitzHugh-Nagumo model. *Physica D* 1984;14:117–124
29. Ermakova EA, Pertsov AM, Shnol EE: On the interaction of vortices in two-dimensional active media. *Physica D* 1989;40: 185–195
30. Zykov VS: *Simulation of Wave Processes in Excitable Media.* New York, Manchester University Press, 1987
31. Courtemanche M, Skaggs W, Winfree A: Stable three dimensional action potential circulation in the FitzHugh-Nagumo model. *Physica D* 1990;41:173–182
32. Delgado C, Steinhaus B, Delmar M, Chialvo D, Jalife J: Directional differences in excitability and margin of safety for propagation in sheep ventricular epicardial muscle. *Circ Res* 1990;67: 97–110
33. Chen PS, Wolf PD, Dixon EG, Danieley ND, Frazier DW, Smith WM, Ideker RE: Mechanism of ventricular vulnerability to single premature stimuli in open chest dogs. *Circ Res* 1988;62:1191–1209
34. Delmar M, Michaels DC, Johnson T, Jalife J: Effects of increasing intracellular resistance on transverse and longitudinal propagation in sheep epicardial muscle. *Circ Res* 1987;60:780–785
35. Spach M, Dolber PC: The relation between propagation in anisotropic cardiac muscle and the "vulnerable period" of reentry, in Zipes DP, Jalife J (eds): *Cardiac Electrophysiology and Arrhythmias.* New York, Grune & Stratton, Inc, 1985, pp 241–252
36. Rudenko AN, Panfilov AV: Drift and interaction of vortices in two-dimensional heterogeneous active medium. *Studia Biophysica* 1983;98:183–188
37. Pertsov AM, Ermakova EA: Mechanism of the drift of spiral wave in an inhomogeneous medium. *Biophysics* 1988;33:338–341
38. Moe GK, Rheinbolt WC, Abildskov JA: A computer model of atrial fibrillation. *Am Heart J* 1964;67:338–356
39. Wiener N, Rosenblueth A: The mathematical formulation of the problem of conduction of impulses in a network of connected excitable elements, specifically in cardiac muscle. *Arch Inst Cardiol Mex* 1946;16:1–61
40. Gerhardt M, Schuster H, Tyson JJ: A cellular automation model of excitable media including curvature and dispersion. *Science* 1990; 247:1563–1566
41. Fast VG, Efimov IG, Krinsky VI: Transition from circular to linear rotation of a vortex in an excitable cellular medium. *Phys Lett A* 1990;151:157–161
42. Roberge FA, Vinet A, Victorri B: Reconstruction of propagated electrical activity with a two-dimensional model of anisotropic heart muscle. *Circ Res* 1986;58:461–475
43. Courtemanche M, Winfree AT: Re-entrant rotating waves in a Beeler-Reuter based model of two-dimensional cardiac conduction. *Int J Bif Chaos* 1991;1:431–444
44. Spach MS, Dolber PC, Heliage JF: Resolution of discontinuous versus continuous propagation: Microscopic mapping of the derivatives of extracellular potential waveforms, in Zipes DP, Jalife J (eds): *Cardiac Electrophysiology: From Cell to Bedside.* Philadelphia, WB Saunders Co, 1990, pp 139–148
45. Spear JF, Balke CW, Lesh MD, Kadish AH, Levine JL, Moore NE: Effect of cellular uncoupling by heptanol on conduction in infarcted myocardium. *Circ Res* 1990;66:202–217
46. Clerc L: Directional differences of impulse spread in trabecular muscle from mammalian heart. *J Physiol* (Lond) 1976;255:335–346
47. Cardinal R, Vermeulen M, Shenasa M, Roberge F, Page P, Hélie F, Savard P: Anisotropic conduction and functional dissociation of ischemic tissue during reentrant ventricular tachycardia in canine myocardial infarction. *Circulation* 1988;77:1162–1176
48. Salama G, Lombardi R, Elson J: Maps of optical action potentials and NADH fluorescence in intact working hearts. *Am J Physiol* 1987;252:H384–H394

49. Salama G, Morad M: Merocyanine 540 as an optical probe of transmembrane electrical activity in the heart. *Science* 1976;191: 485–487
50. Li T, Sperelakis N, Teneick RE, Solaro JR: Effects of diacetyl monoxime on cardiac excitation-contraction coupling. *J Pharmacol Exp Ther* 1985;232:688–695
51. Gwathmey JK, Hajjar RJ, Solaro RJ: Contractile deactivation and uncoupling of crossbridges: Effects of 2,3-butanedione monoxime on mammalian myocardium. *Circ Res* 1991;69:1280–1292
52. Gul'ko FB, Petrov AA: Mechanism of the formation of closed pathways of conduction in excitable media. *Biophysics* 1972;17: 261–270
53. Winfree A: Estimating the ventricular fibrillation threshold, in Glass L, Hunter P, McCulloch A (eds): *Theory of Heart.* New York, Springer-Verlag New York, Inc, 1991, pp 477–532
54. El-Sherif N, Smith A, Evans K: Canine ventricular arrhythmias in the late myocardial infarction period: 8. Epicardial mapping of reentrant circuits. *Circ Res* 1981;49:255–265
55. Fast VG, Pertsov AM: Drift of a vortex in the myocardium. *Biophysics* 1990;35:489–494
56. Yermakova YA, Pertsov AM: Interaction of rotating spiral waves with a boundary. *Biophysics* 1986;31:932–940
57. Kadish AH, Morady F: Torsades de pointes, in Zipes DP, Jalife J (eds): *Cardiac Electrophysiology: From Cell to Bedside.* Philadelphia, WB Saunders Co, 1990, pp 605–610
58. Dessertenne F: La tachycardie ventriculaire à deux foyers opposés variable. *Arch Mal Coer* 1966;56:263–272
59. Jackman WM, Friday KJ, Anderson JL, Aliot EM, Clark M, Lazzara R: The long QT syndromes: A critical review, new clinical observations and a unifying hypothesis. *Prog Cardiovasc Dis* 1988; 31:115–172
60. Winfree AT: Electrical instability in cardiac muscle: Phase singularities and rotors. *J Theor Biol* 1989;138:353–405
61. Abildskov JA, Lux RL: The mechanism of simulated torsades de pointes in computer model of propagated excitation. *J Cardiovasc Electrophysiol* 1991;2:224–237
62. D'Alnoncourt N, Zierhut, B Lüderitz: "Torsades de pointes" tachycardia: Re-entry or focal activity? *Br Heart J* 1982;48: 213–216